SKOR1 mediates FER kinase-dependent invasive growth of breast cancer cells

Sluimer, L.M.; Bullock, E.; Rätze, M.A.K.; Enserink, L.; Overbeeke, C.; Hornsveld, M.; ... ; Tavares, S.

© 2023. Published by The Company of Biologists Ltd | Journal of Cell Science (2023) 136, jcs260243. doi:10.1242/jcs.260243

RESEARCH ARTICLE

SKOR1 mediates FER kinase-dependent invasive growth of breast cancer cells

Lilian M. Sluimer[1], Esme Bullock[2], Max A. K. Rätze[1], Lotte Enserink[1], Celine Overbeeke[1], Marten Hornsveld[3], Valerie G. Brunton[2], Patrick W. B. Derksen[1,*] and Sandra Tavares[1,4,5,*]

ABSTRACT

High expression of the non-receptor tyrosine kinase FER is an independent prognostic factor that correlates with poor survival in breast cancer patients. To investigate whether the kinase activity of FER is essential for its oncogenic properties, we developed an ATP analogue-sensitive knock-in allele (FER^{ASKI}). Specific FER kinase inhibition in MDA-MB-231 cells reduces migration and invasion, as well as metastasis when xenografted into a mouse model of breast cancer. Using the FER^{ASKI} system, we identified Ski family transcriptional corepressor 1 (SKOR1) as a direct FER kinase substrate. SKOR1 loss phenocopies FER inhibition, leading to impaired proliferation, migration and invasion, and inhibition of breast cancer growth and metastasis formation in mice. We show that SKOR1 Y234, a candidate FER phosphorylation site, is essential for FER-dependent tumor progression. Finally, our work suggests that the SKOR1 Y234 residue promotes Smad2/3 signaling through SKOR1 binding to Smad3. Our study thus identifies SKOR1 as a mediator of FER-dependent progression of high-risk breast cancers.

KEY WORDS: Breast cancer, FER tyrosine kinase, SKOR1, Metastasis, Analogue-sensitive, CRISPR-Cas9

INTRODUCTION

Metastasis underlies the mortality in most high-grade and triple-negative breast cancer (TNBC) patients (Kirsch and Loeffler, 2005). Clinical management of these aggressive breast cancer types is challenging owing to a lack of responses to standard chemotherapy treatment and regimens using hormone receptor antagonists (Aversa et al., 2014; Kennecke et al., 2010). Together, these features underscore an unmet need: the identification of markers that identify drug benefit and/or allow targeted intervention of high-risk breast cancers.

The FPS/FES-related non-receptor tyrosine kinase FER was identified as a promising candidate for targeted therapy of metastatic breast cancer (Ivanova et al., 2013; Tavares et al., 2022). Yet, caveats in using such an approach rely on the role of FER in regulating normal inflammation and innate immunity (Craig and Greer, 2002), and on the inexistence of specific FER inhibitors. The FER kinase regulates cell–cell and cell–matrix contacts, possibly through interaction with the adherens junction components p120-catenin and β-catenin (Greer, 2002), by controlling actin polymerization (Ladwein and Rottner, 2008) or through downregulating the synthesis of glycans that bind to the basement membrane protein laminin (Yoneyama et al., 2012). Moreover, FER controls cell cycle progression and promotes integrin-dependent cell migration and invasion (Arregui et al., 2000; Ivanova et al., 2013; Kapus et al., 2000; Kim and Wong, 1995). High FER levels have been linked to ovarian, renal and colon cancer progression (Allard et al., 2000; Kawakami et al., 2013; Li et al., 2009; Menges et al., 2010; Takeshima et al., 1998; Zirngibl et al., 2001). In breast cancer, FER expression is an independent predictor of survival, especially in lymph-node-negative patients (Ivanova et al., 2013). Elevated FER levels correlate with high-grade breast cancer types, such as TNBC and breast cancer brain metastasis (Ivanova et al., 2013; Oshi et al., 2020). Moreover, FER promotes the growth and dissemination of melanoma and breast cancer cells in mouse models (Ivanova et al., 2013, 2019). Apart from tyrosine phosphorylation of p120-catenin, β-catenin, the actin-binding protein cortactin (Kim and Wong, 1998) and the microtubule interactor CRMP2 (Zheng et al., 2018), functional data on direct FER substrates are currently scarce and limited to its substrates DCTN2 and MAPK1 (Tavares et al., 2022).

Sno/Ski family members have been linked to the transforming growth factor β (TGFβ) and bone morphogenic protein (BMP) signaling pathways, possibly through binding and antagonizing Smad proteins (Akiyoshi et al., 1999; Luo, 2004; Luo et al., 1999). Although Sno and Ski are classified as proto-oncogenes, their exact role in tumor progression remains largely unknown. All Sno/Ski family members feature a conserved SAND (Sp100, AIRE-1, NucP41/75, DEAF-1) motif within their Ski homology domain (Wu et al., 2002). The SAND domain is present in a subset of nuclear proteins that are involved in chromatin-dependent transcriptional regulation (Bottomley et al., 2001). An interaction loop (I-loop) within the SAND domain allows these proteins to bind DNA (Bottomley et al., 2001; Wu et al., 2002). In addition, it has been described that Ski, SnoN and SKOR2 can interact with Smad2/3 through their N-terminal regions and with Smad4 through their SAND domains (Wu et al., 2002).

SKOR1, or functional Smad-suppressing element on chromosome 15 (Fussel-15), is the most recently identified member of the Sno/Ski family (Arndt et al., 2007). Human SKOR1 is primarily, but not exclusively, expressed in the central nervous system in the migratory precursors of cerebellar Purkinje cells (Arndt et al., 2007). SKOR1 can act as a transcriptional

[1]Department of Pathology, University Medical Center Utrecht, Heidelberglaan 100, 3584 CX Utrecht, The Netherlands. [2]Edinburgh Cancer Research UK Centre, University of Edinburgh, Crewe Road South, EH4 2XR Edinburgh, UK. [3]Department of Molecular Cell Biology, Cancer Genomics Centre Netherlands and Centre for Biomedical Genetics, Leiden University Medical Center, Einthovenweg 20, 2333 ZC Leiden, The Netherlands. [4]i3S - Instituto de Investigação e Inovação em Saúde, Universidade do Porto, Rua Alfredo Allen 208, 4200-135 Porto, Portugal. [5]IPATIMUP - Instituto de Patologia e Imunologia Molecular da Universidade do Porto, Rua Júlio Amaral de Carvalho 45, 4200-135 Porto, Portugal.

*Authors for correspondence (stavares@ipatimup.pt; p.w.b.derksen@umcutrecht.nl)

C.O., 0000-0003-3877-7328; V.G.B., 0000-0002-7778-8794; P.W.B.D., 0000-0003-0732-7762; S.T., 0000-0003-3055-914X

Handling Editor: Andrew Ewald
Received 17 May 2022; Accepted 22 December 2022

Journal of Cell Science (2023) 136, jcs260243. doi:10.1242/jcs.260243

co-repressor with the homeodomain transcription factor Lbx1, thereby regulating the cell fate of dorsal horn interneurons (Mizuhara et al., 2005). Recent evidence suggests a role for SKOR1 in restless leg syndrome and in the transcriptional regulation of genes involved in neurodevelopment and iron metabolism (Sarayloo et al., 2020). Additionally, activated fibroblasts express SKOR1 during the early phases of wound healing, where it promotes fibroblast migration and affects F-actin and focal adhesion distribution (Arndt et al., 2011). Moreover, the *Drosophila* homologue of SKOR1, Fuss, inhibits differentiation and sustains proliferation in developing eye imaginal discs (Rass et al., 2022). In cancer, functions for SKOR1 have remained largely unexplored, except for a recent study observing SKOR1 expression in breast cancer metastasis to the brain (Oshi et al., 2020).

Based on a chemical genetics approach, we have identified and validated SKOR1 as a direct substrate of the non-receptor tyrosine kinase FER. Our data demonstrate that SKOR1 is essential for tumor growth and invasion, functions that are dependent on the tyrosine residue Y234 in SKOR1, a candidate FER phosphorylation site.

RESULTS

FER kinase activity controls invasion and metastasis formation in TNBC

Previous studies have established FER as a driver of invasion and metastasis formation in high-grade and basal-like breast cancers (Ivanova et al., 2013). To study whether FER relies on its kinase activity to drive tumor progression, we generated a FER analogue-sensitive (FER-AS) knock-in allele (FER^{ASKI}) in MDA-MB-231 (MM231) cells using CRISPR–Cas9 gene editing (Fig. S1A–D). To do so, the gatekeeper residue in the kinase-active site of endogenous FER was mutated, which results in an enlarged ATP-binding pocket (Tavares et al., 2022). Mutation of methionine 637 to alanine (M637A) in FER confers unique sensitivity to chemically modified derivatives of PP1, a Src-family-selective inhibitor (Bishop et al., 1999, 2000). Knock-in of the gatekeeper mutation (M637A) results in near-endogenous expression levels of FER-AS in MM231 parental cells (Fig. S1E). Importantly, analogue-sensitive kinase inhibition using the PP1 analogue kinase inhibitor 1-(1,1-dimethylethyl)-3-(1-naphthalenylmethyl)-1H-pyrazolo(3,4-d) pyrimidin-4-amine (NM-PP1) does not influence expression of FER-AS (Fig. S1E), but leads to decreased tyrosine phosphorylation on several proteins (Fig. S1F). Whereas no effect is observed in control MM231 cells (Fig. S1G–J) (Tavares et al., 2022), treatment of FER^{ASKI} cells with 1 µM NM-PP1 leads to a spread and sessile phenotype accompanied by abundant stress fibers and focal adhesion (FA) formation (Fig. 1A,B), indicating that this phenotype is a result of the specific inhibition of FER kinase activity. Additionally, we observed no significant changes in the activation of other tyrosine kinases, such as Src, upon treatment of NM-PP1 on parental MM231 cells (Fig. S1K). As loss of FER was shown to inhibit cell cycle progression and impair proliferation of MM231 cells (Ivanova et al., 2013; Pasder et al., 2006), we further explored the role of its kinase activity in regulating TNBC cell proliferation. FER kinase inhibition in FER^{ASKI} interphase cells using NM-PP1 resulted in a modest but not significant decrease in proliferation (Fig. S1J). As a control, we treated MM231 doxycycline (DOX)-inducible FER knockdown (FER iKD) cells (cultured in the presence or absence of DOX) with or without NM-PP1 and observed neither differences in FER protein levels nor a significant reduction in proliferation (Fig. S1I,L,M). Importantly, however, addition of NM-PP1 impaired cell motility in 2D (Fig. 1C). Although proliferation was not significantly affected upon specific FER kinase inhibition in three-dimensional (3D) cultured cells (Fig. 1D; quantified in Fig. S1N), invasion was significantly impaired upon treatment with NM-PP1 (Fig. 1D,E). Taken together, these results provide formal evidence that FER regulates tumor cell invasion and migration through its tyrosine kinase activity.

Although FER depletion is sufficient to inhibit metastasis formation of MM231 cells in mice (Ivanova et al., 2013), it remained unclear whether this was due to inhibition of its tyrosine kinase activity. To test this, we orthotopically transplanted luciferase-tagged FER^{ASKI} cells in recipient immune-deficient mice and started treatment with NM-PP1 upon formation of palpable primary tumors (~50 mm^3). Tumor growth was monitored longitudinally, and mice were euthanized once lung metastases were detected by bioluminescence imaging. We did not observe differences in primary tumor volumes between the treated and untreated cohorts (Fig. 1F; quantified in Fig. S1O), in agreement with published findings showing that loss of FER function *in vivo* mainly affects invasion and metastasis (Ivanova et al., 2013). Untreated animals showed a median metastasis-free latency of approximately 22 days (Fig. 1G), supporting published findings using FER loss (Ivanova et al., 2013) and showing that the FER^{ASKI} allele is fully functional *in vivo*. In contrast, inhibition of FER kinase activity with NM-PP1 delayed the median development of metastasis to 28 days compared to the control group (P=0.006; Fig. 1G). NM-PP1-treated mice developed tumors that showed reduced local invasion in the surrounding tissue compared to control mice (Fig. 1H). Taken together, these results demonstrate that FER kinase activity promotes tumor invasion and metastasis of TNBC cells in mice.

To analyze the impact of FER on phosphorylated downstream effectors, we used a FER iKD combined with reverse-phase protein array (RPPA) analysis (Fig. S2A, Fig. S3A). Expression and phosphorylation were assayed using stable FER iKD in two high-grade basal breast cancer cell types, MM231 (Fig. S2B; Table S1) and SUM149PT (Fig. S3B; Table S2). The changes observed in a range of signaling proteins and phosphoproteins upon FER iKD in MM231 and SUM149PT cells demonstrate that FER drives crucial signaling pathways in both cell types. DOX-induced loss of FER expression attenuated the activation of multiple key signaling pathways in MM231 cells (Table S1), such as Rb (or RB1) phosphorylation at S807 and S780 (Fig. S2C), which is required for the G0–G1 transition (Ren and Rollins, 2004). In line with the kinase-specific inhibition of FER (Fig. S1F), we found that EGFR Y1173 phosphorylation was reduced upon loss of FER in MM231 cells (Table S1), confirming EGFR as a FER downstream target (Guo and Stark, 2011; Tavares et al., 2022). Moreover, we observed altered levels of VEGFR2 Y1175, PDGFRB Y1021 and IGF1R Y1162/1163 phosphorylation upon FER loss (Tables S1 and S2), suggesting that FER indirectly controls the function and/or processing of multiple growth factor receptors. Interestingly, Smad2/3 phosphorylation levels were consistently decreased after FER loss on several serine epitopes in both cell systems used (Tables S1 and S2), which suggests a role for the regulation of TGFβ/BMP signals by FER.

SKOR1 is a direct FER substrate that promotes migration and invasion

We have recently performed chemical genetics (Bishop et al., 2000) using a truncated version of FER-AS to identify direct FER kinase substrates (Tavares et al., 2022). From these targets we selected SKOR1, a Sno/Ski family member that is classified as a proto-oncogene. SKOR1 was selected because it has been linked to the

Journal of Cell Science (2023) 136, jcs260243. doi:10.1242/jcs.260243

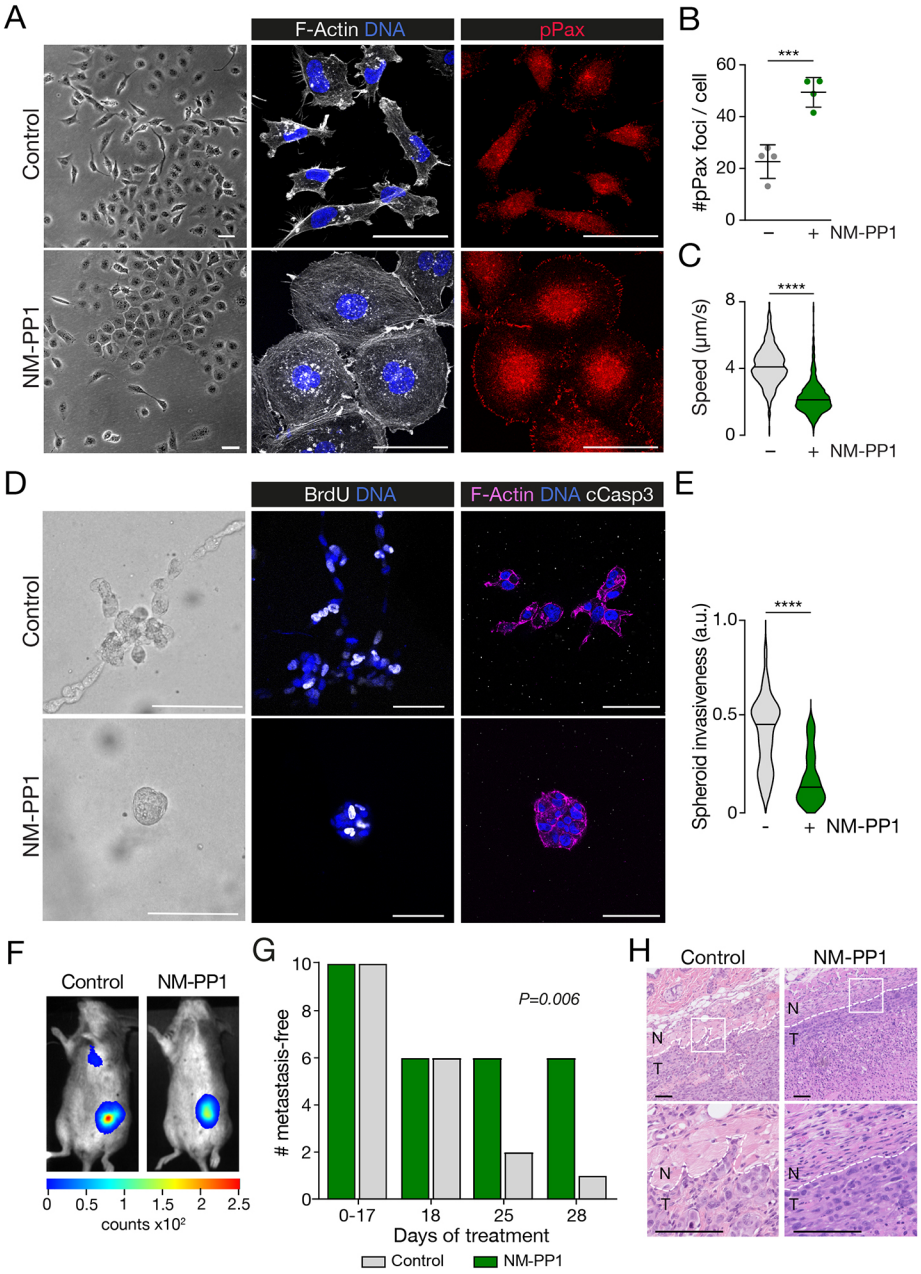

Fig. 1. FER kinase activity promotes cell migration and invasion. (A–C) Inhibition of FER-AS kinase using NM-PP1 induces cell spreading, stress fiber formation and focal adhesion (FA) formation, and reduces motility in MM231 cells. Cells were imaged by phase-contrast microscopy (A) and stained for F-actin (middle panel, white), DNA (DAPI, middle panel, blue) and phospho-Pax (pPax, right panel, red). Scale bars: 50 µm. Quantifications of pPax foci in FER^{ASKI} cells treated with NM-PP1 (n=65) or without NM-PP1 (n=43) are shown in B. Quantifications are from at least three independent experiments. Migration speed was quantified in C using live fluorescence imaging of MM231 FER^{ASKI} cells treated with control (n=4815) or with NM-PP1 (n=4171). Quantifications are from three independent experiments. (D,E) FER kinase is essential for 3D invasion. FER^{ASKI} cells were plated in BME as tumor spheroids, treated with NM-PP1 and imaged by phase-contrast microscopy or for BrdU incorporation (middle panel, white), cleaved caspase-3 (right panel, white), F-actin (right panel, magenta) and DNA (DAPI, blue). Scale bars: 50 µm. The quantification of invasiveness of tumor spheroids treated with DMSO (n=36) or NM-PP1 (n=43) is shown in E. Error bars denote s.d. ***P<0.001; ****P<0.0001; unpaired two-tailed t-test. a.u., arbitrary units. (F,G) Inhibition of FER kinase activity prolongs metastasis-free survival in mice. FER^{ASKI} cells were xenografted, and tumor volume and metastasis formation were monitored upon administration of DMSO (control, n=10) or NM-PP1 (n=10). Metastasis was determined by lung bioluminescence or post-mortem assessment of lung metastatic foci. Representative images of mice treated with control or NM-PP1 at end points are shown in F. Survival of mice upon treatment is shown in G. Statistical analysis of survival distributions for the different treatments was performed using the log-rank (Mantel–Cox) test. (H) FER kinase activity regulates tumor invasion. Dashed white lines indicate the tumor (T)–normal (N) breast tissue border. Inset images correspond to a 200% magnification. Scale bars: 100 µm.

regulation of BMP signaling through interaction with Smad proteins (Arndt et al., 2007; Gray et al., 2019), its expression has been observed in breast cancer brain metastases (Oshi et al., 2020) and its role in tumor progression remains largely unknown. We validated SKOR1 as a direct FER substrate *in vitro* using a fusion protein containing GST and SKOR1 exon 5, and ATP incorporation (Fig. 2A,B). SKOR1 phosphorylation was specific, because using either a kinase-dead FER (D742R) or pharmacological inhibition of the gatekeeper FER kinase using NM-PP1 significantly inhibited SKOR1 phosphorylation (Fig. 2A,B). Moreover, phosphorylation was reduced when using SKOR1-Y^{NULL}, a SKOR1 mutant in which all tyrosine residues in exon 5 are mutated to alanine (Fig. S4A), indicating that FER-dependent phosphorylation occurs specifically on tyrosine residues.

To analyze the role of SKOR1 in high-grade metastatic breast cancer cells, we performed a stable knockdown of SKOR1 in MM231 using two independent shRNA hairpins (Fig. 2C–E). *SKOR1* mRNA levels were stably and consistently reduced to approximately 50% in multiple independent experiments (Fig. 2C). Reducing SKOR1 levels using either hairpin resulted in a stark reduction in cell numbers compared to cells treated with the scrambled control shRNA (compare day 1 to day 4, Fig. S4B), suggesting that SKOR1 is necessary for cell proliferation and survival. After stable integration and selection, we confirmed that SKOR1-depleted cells displayed a decreased proliferative capacity (Fig. 2E). Strikingly, loss of SKOR1 phenocopied FER depletion (Ivanova et al., 2013) and inhibition (Fig. 1A, Fig. 2D), including extensive cell spreading and collective growth as non-motile cells. SKOR1 depletion also induced loss of lamellipodia and F-actin stress fiber formation in 2D (Fig. 2D), a characteristic feature of FER loss or inhibition in MM231 cells (Ivanova et al., 2013) (Fig. 1A).

To temporally and reversibly control the SKOR1 knockdown, we employed a DOX-inducible lentiviral shRNA system in MM231

Journal of Cell Science

Journal of Cell Science (2023) 136, jcs260243. doi:10.1242/jcs.260243

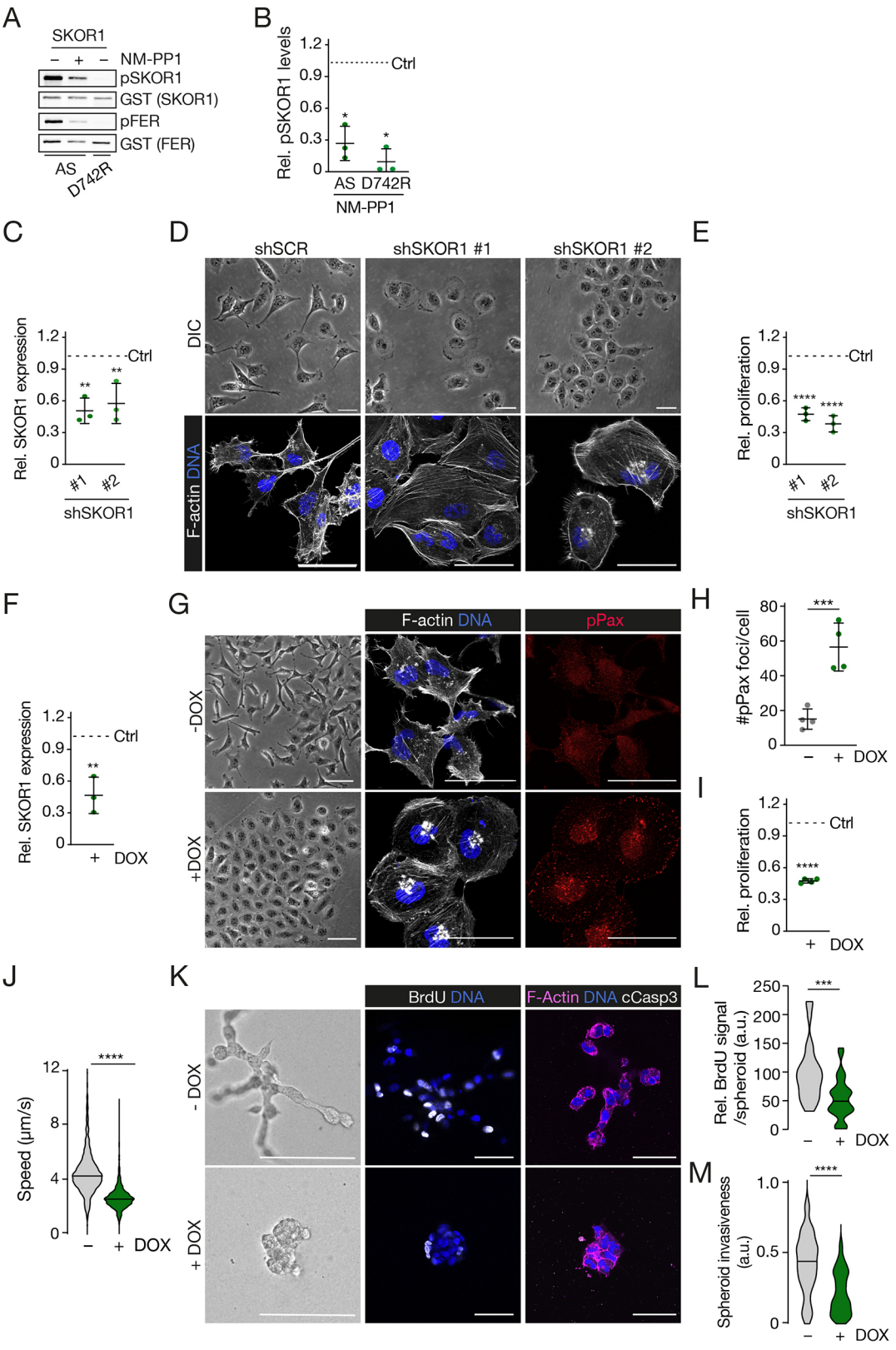

Fig. 2. See next page for legend.

and SUM149PT cells, which reproducibly resulted in a 50% reduction of SKOR1 expression after induction (SKOR1 iKD) (Fig. 2F; Fig. S5A). Inducible SKOR1 loss caused extensive cell spreading, formation of stress fibers (Fig. 2G; Fig. S5B) and a significant increase in FA formation (Fig. 2H; Fig. S5C). In addition, we observed that SKOR1 knockdown led to impaired two-dimensional (2D) proliferation of MM231 cells (Fig. 2I) and impairment of single-cell migration compared to cells cultured in

Journal of Cell Science

Journal of Cell Science (2023) 136, jcs260243. doi:10.1242/jcs.260243

Fig. 2. SKOR1 is a FER kinase substrate that promotes breast cancer cell proliferation and invasion. (A,B) FER phosphorylates SKOR1 *in vitro*. Kinase assay using recombinant GST–analog sensitive FER (AS) or GST–kinase-dead FER (D742R) in the presence of N-benzyl (Bn)-ATPγS, with (+) or without (–) NM-PP1. GST-tagged SKOR1^{WT} was used as the substrate. Thio-phosphorylated proteins were detected with a thiophosphate ester epitope-specific antibody. Auto-thio-phosphorylation of FER served as a positive control. GST-FER was used as the loading control. Depicted are the fold changes of the thio-phosphorylated FER (AS) or GST-kinase-dead FER (D742R) protein levels from at least three independent experiments compared to the control samples (Ctrl, dashed line) (B). (C,D,F–H) SKOR1 is critical for TNBC cell morphology in 2D. Validation of SKOR1 knockdown using real-time qPCR amplification in stable (C) and DOX-inducible (F) KD cells. Relative fold changes of SKOR1 expression compared to control samples (Ctrl, dashed line) in stable (C) and DOX-inducible (F) KD cells were quantified from three independent experiments. MM231 stable SKOR1 KD cells were imaged using phase-contrast microscopy (upper panel) or for F-actin (lower panel, white) and DNA (DAPI, blue) (D). MM231 SKOR1 iKD cells were treated with DOX and imaged by phase-contrast microscopy (left panel) or for F-actin (middle panel, white), pPax (right panel, red) and DNA (DAPI, blue) (G). Scale bars: 50 µm. Quantifications of pPax foci in SKOR iKD cells treated with (*n*=87) or without DOX (*n*=71) are shown in H. Note the cell spreading, stress fiber formation and increase in FA formation upon SKOR1 loss. (E,I) SKOR1 controls TNBC cell proliferation. Relative fold changes of cell proliferation compared to control samples (Ctrl, dashed line) were quantified in stable (E) and DOX-inducible (I) SKOR1 KD cells using colony formation assays. (J) SKOR1 is important for 2D cell motility. Migration speed was quantified using live fluorescence imaging of MM231 SKOR1 iKD cells transfected with pGK-GFP (Cellomics Technology, PLV-10077-50), treated with (*n*=6136) or without DOX (*n*=6870) and grown in 2D. Quantifications are from three independent experiments. (K–M) SKOR1 is required for proliferation and invasion in 3D. MM231 SKOR1 iKD cells were treated with DOX and plated in BME to form 3D spheres. Cells were imaged by phase-contrast microscopy or for BrdU (middle panel, white), cleaved caspase-3 (right panel, white), F-actin (right panel, magenta) and DNA (DAPI, blue). Scale bars: 50 µm. Quantification of BrdU positive nuclei of SKOR1 iKD spheroids treated with (*n*=28) or without DOX (*n*=29) is shown in L. Quantification of spheroid invasion of SKOR1 iKD spheroids treated with (*n*=47) or without DOX (*n*=38) is shown in M. Error bars denote s.d. a.u., arbitrary units. **P*<0.05; ***P*<0.01; ****P*<0.001; *****P*<0.0001; unpaired two-tailed *t*-test.

control conditions for both the MM231 and SUM149PT cell lines (Fig. 2J; Fig. S5D).

We next cultured MM231 SKOR1 iKD cells in 3D basement membrane extract gels and observed that SKOR1 depletion fully prevented invasion, compared to control spheroids that exhibited highly branched, invasive and disorganized colonies (Fig. 2K,M). Because SKOR1-depleted cells showed clear growth defects when cultured in 2D, we assessed proliferation and apoptosis using bromodeoxyuridine (BrdU) incorporation and cleaved caspase-3 as markers, respectively. These analyses indicated that the reduction in colony formation upon SKOR1 depletion was mainly due to an impairment in proliferation in 3D (Fig. 2L) because we observed no differences in apoptosis compared to controls (Fig. 2K).

SKOR1 Y234 is required for cellular proliferation and invasion

Our chemical genetics and proteomics studies identified SKOR1 Y234 as a candidate FER phosphorylation site, a residue that resides in the I-loop of the SAND domain (Fig. 3A) (Arndt et al., 2007). We therefore stably expressed a GFP-tagged and RNAi-resistant wild-type (WT) SKOR1 cDNA or a SKOR1 cDNA harboring a phenylalanine at position 234 (Y234F) in MM231 SKOR1 iKD cells (SKOR1^{RECON}) (Fig. 3B), which prevents phosphorylation of SKOR1 Y234 without altering the protein structure. Upon SKOR1 reconstitution, we observed that the WT cDNA fully rescued the SKOR1 knockdown phenotype, presenting a migratory and spindle-like morphology resembling the parental MM231 morphology (Fig. 3C, upper panels). Conversely, SKOR1^{RECON} SKOR1^{Y234F} cells failed to migrate and exhibited a spread and sessile phenotype (Fig. 3C, bottom panels). Impairment of migration in SKOR1^{RECON} SKOR1^{Y234F} cells coincided with the formation of stress fibers and a marked increase in the number of FA sites (Fig. 3C; quantified in Fig. 3D), suggesting that the SKOR1 Y234 residue is involved in the regulation of F-actin dynamics and FA formation in MM231 cells. In line with these observations, overexpressing SKOR1^{WT} in control cells did not affect migration or FA dynamics, whereas overexpressing SKOR1^{Y234F} in control cells reduced migration and disturbed FA dynamics compared to control or SKOR1^{WT}-overexpressing cells (Fig. S6B–D). These results suggest that high expression of SKOR1^{Y234F} is sufficient to overtake or interfere with the role of endogenous SKOR1 in regulating cell migration and FA organization.

SKOR1^{WT} and SKOR1^{Y234F} localized throughout the cytosol in vesicular-like structures that are most prominent in the perinuclear region (Fig. 3C; Fig. S6B). Interestingly, reconstitution with SKOR1^{Y234F} resulted in a 60% decrease in cellular proliferation in 2D compared to reconstitution with SKOR1^{WT} (Fig. 3E). Next, we assessed 3D cancer cell invasion, proliferation and apoptosis. We unexpectedly observed that the SKOR1 Y234 residue did not significantly contribute to either cellular proliferation or apoptosis in this setting (Fig. 3F,G). However, the SKOR1^{Y234F} mutant was unable to rescue the invasion of MM231 cells in 3D (Fig. 3F; quantified in Fig. 3H). Taken together, our results show that SKOR1 Y234, a candidate FER phosphorylation site, is necessary for the invasion of the triple-negative MM231 cells.

Because of the overlap in phenotype upon inhibition of FER kinase activity with NM-PP1 or depleting SKOR1, we used the FER^{ASKI} model and transduced SKOR1^{WT} or SKOR1^{Y234F} to assess functional interdependence. Control FER^{ASKI} SKOR1^{WT} cells displayed a highly invasive phenotype, with lamellipodium formation and spindle-shaped cells (Fig. 4A). SKOR1^{WT} fully prevented the phenotypical consequences of FER kinase inactivation in the presence of NM-PP1, sustaining a spindle-like and motile cell phenotype with sparse FA sites (Fig. 4A, bottom panels; Fig. 4B). Control FER^{ASKI} SKOR1^{Y234F} cells exhibited a mixed or hypomorphic phenotype, wherein migratory cells coincided with cells that showed extensive cell spreading and an increase in FA formation (Fig. 4A,B). Inhibition of FER kinase activity using NM-PP1 induced a further increase in cell spreading and an accompanying transition from a spindle-like cell shape to a spread phenotype with an increased number of FA sites in FER^{ASKI} SKOR1^{Y234F} cells (Fig. 4A,B). Overexpression of SKOR1^{WT} in NM-PP1-treated FER^{ASKI} cells resulted in a minor but not significant increase in cell proliferation in 2D (Fig. 4C), suggesting a compensatory effect of SKOR1^{WT} overexpression when FER kinase activity was reduced. Interestingly, proliferation defects were observed in FER^{ASKI} SKOR1^{Y234F} cells treated with NM-PP1 (Fig. 4C), indicating that SKOR1 Y234 is involved in TNBC cell proliferation.

We also studied the effect of the SKOR1 Y234 residue on 3D invasion in the context of FER kinase function and observed that SKOR1^{Y234F}, in contrast to SKOR1^{WT}, was unable to rescue the impaired invasive growth caused by FER inactivation (Fig. 4D). Treatment with NM-PP1 led to a full inhibition of both invasion and proliferation in FER^{ASKI} SKOR1^{Y234F} cells, whereas FER^{ASKI} SKOR1^{WT} cells formed highly invasive structures upon NM-PP1 treatment (Fig. 4D–F). These data suggest that the SKOR1^{Y234} residue functions downstream of the FER kinase to promote tumor cell proliferation and invasion of high-grade breast cancer cells.

Journal of Cell Science (2023) 136, jcs260243. doi:10.1242/jcs.260243

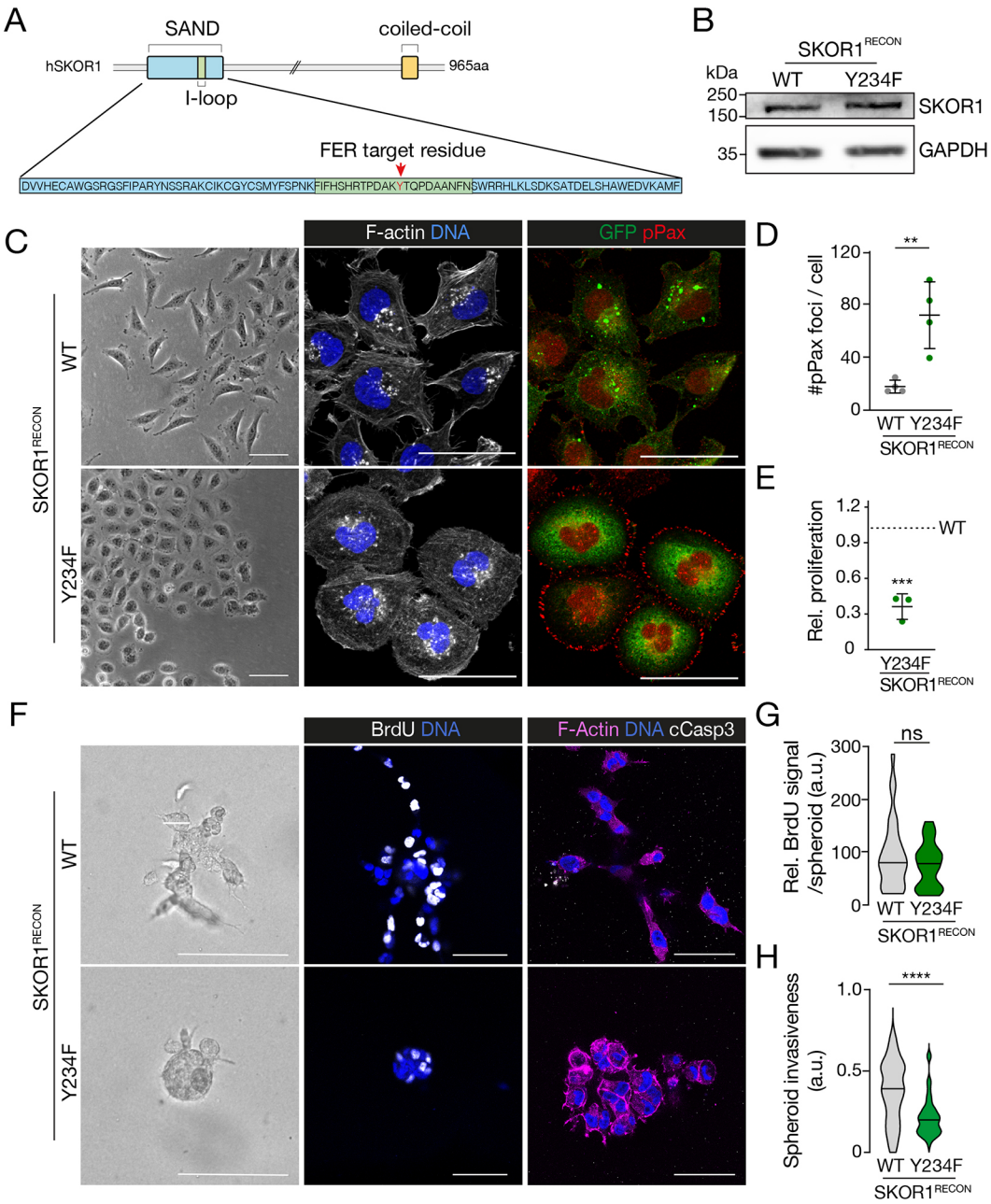

Fig. 3. SKOR1 Y234 is required for cell motility and invasion. (A) The FER target residue of SKOR1 resides in the I-loop of the SAND domain. A schematic of human SKOR1 domains is shown. (B–H) MM231 SKOR1 iKD cells were reconstituted (SKOR1^{RECON}) with either SKOR1 wild-type (SKOR1^{WT}) or a SKOR1 mutant in which Y234 was substituted for phenylalanine (SKOR1^{Y234F}). SKOR1^{WT} and SKOR1^{Y234F} are equally expressed (B), as determined by western blotting. GAPDH was used as a loading control. (C–E) The SKOR1 Y234 residue is required for motility, invasion and proliferation. Cells were stained for F-actin (middle panel, white), pPax (right panel, red) and DNA (DAPI, blue) (C). Scale bars: 50 µm. Note the extensive cell spreading and increase in the number of pPax foci in SKOR1^{Y234F} cells, as well as the cytoplasmic localization of SKOR1 in the WT and Y234F-reconstituted cells (right panel). Quantifications of FA formation in SKOR1^{WT} cells (n=56) or SKOR1^{Y234F} cells (n=63) are shown in D. Quantifications are from three independent experiments. The relative fold change of cell proliferation compared to control samples (WT, dashed line) was quantified using colony formation assays (E). (F–H) SKOR1 Y234 regulates 3D invasion. SKOR1^{WT}- or SKOR1^{Y234F}-reconstituted cells were plated in BME as tumor spheroids. Cells were imaged by phase-contrast microscopy or for BrdU incorporation (middle panel, white), cleaved caspase-3 (right panel, white), F-actin (right panel, magenta) and DNA (DAPI, blue). Scale bars: 50 µm. Quantification of BrdU-positive nuclei of SKOR1^{WT} spheroids (n=30) or SKOR1^{Y234F} spheroids (n=29) is shown in G. Quantification of spheroid invasion of SKOR1^{WT} spheroids (n=44) or SKOR1^{Y234F} spheroids (n=47) is shown in H. Error bars denote s.d. a.u., arbitrary units. ns, not significant; **P<0.01, ***P<0.001; ****P<0.0001; unpaired two-tailed t-test.

SKOR1 regulates BMP/TGFβ signaling and binds Smad2/3 in TNBC cells

We next tested whether SKOR1 Y234 modulation leads to phosphorylation changes in signaling pathways. For this, we used RPPA combined with SKOR1 reconstitution in MM231 SKOR1 iKD cells (Fig. 5A; Table S3). Reconstitution with SKOR1^{Y234F} reduced phosphorylation of EGFR and its downstream effectors such as 4EBP1 (encoded by *EIF4EBP1*) and MAP kinase on multiple epitopes (Fig. 5B, right panel; Table S3). When comparing SKOR1^{Y234F} cells to FER iKD cells, we observed that many

Journal of Cell Science (2023) 136, jcs260243. doi:10.1242/jcs.260243

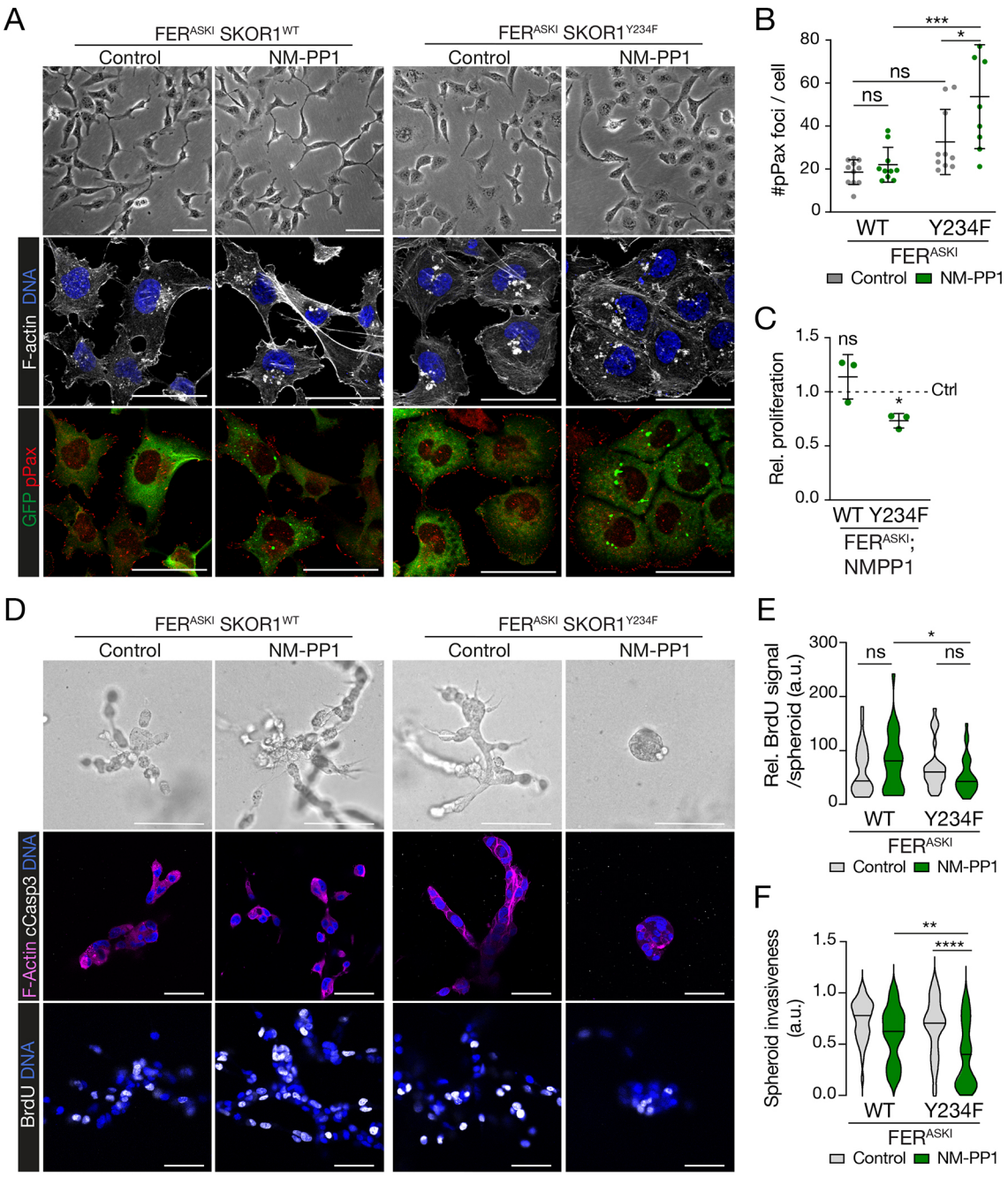

Fig. 4. SKOR1 promotes FER-induced migration and invasion through its Y234 residue. (A–C) SKOR1 Y234 controls FER-induced cell motility and proliferation. MM231 FER^{ASKI} cells expressing SKOR1^{WT} or SKOR1^{Y234F} (green) were imaged by phase-contrast microscopy or for F-actin (middle panel, white), pPax (lower panel, red) and DNA (DAPI). Scale bars: 50 µm. Quantifications from three independent experiments of pPax foci in FER^{ASKI} cells expressing SKOR1^{WT} treated with DMSO (n=129) or NM-PP1 (n=163), or SKOR1^{Y234F} treated with DMSO (n=151) or NM-PP1 (n=121) are shown in B. The relative fold change of cell proliferation compared to control samples (dashed line) was quantified using colony formation assays (C). (D–F) SKOR1 Y234 is critical for FER-induced 3D invasion. MM231 FER^{ASKI} cells expressing SKOR1^{WT} or SKOR1^{Y234F} (green) were cultured in the presence of NM-PP1 and plated in BME as tumor spheroids. Cells were imaged by phase-contrast microscopy or for BrdU incorporation (middle panel, white), cleaved caspase-3 (right panel, white), F-actin (right panel, magenta) and DNA (DAPI, blue) (D). Scale bars: 50 µm. Quantification of BrdU-positive nuclei of FER^{ASKI} spheroids expressing SKOR1^{WT} treated with DMSO (n=30) or NM-PP1 (n=30), or SKOR1^{Y234F} treated with DMSO (n=30) or NM-PP1 (n=30) is shown in E. Quantification of spheroid invasion of FER^{ASKI} spheroids expressing SKOR1^{WT} treated with DMSO (n=36) or NM-PP1 (n=42), or SKOR1^{Y234F} treated with DMSO (n=39) or NM-PP1 (n=41) is shown in F. Error bars denote s.d. a.u., arbitrary units. ns, not significant; *P<0.05; **P<0.01; ***P<0.001; ****P<0.0001; one-way ANOVA with a Sidak post hoc test.

substrates altered by SKOR1^{Y234F} expression were similarly affected by FER depletion, including Rb (S780 and S807), mTOR and EGFR (Y1173) (Fig. 5B). Importantly, like in FER-depleted cells, SKOR1^{Y234F} reconstitution led to a decrease in Smad2/3 phosphorylation (S423, S425 and S467/S425) (Fig. 5B), which is in concordance with reported links of SKOR1 to BMP/TGFβ signaling (Arndt et al., 2007; Fischer et al., 2012; Takaesu et al., 2012). To verify possible ties between SKOR1 and

Journal of Cell Science (2023) 136, jcs260243. doi:10.1242/jcs.260243

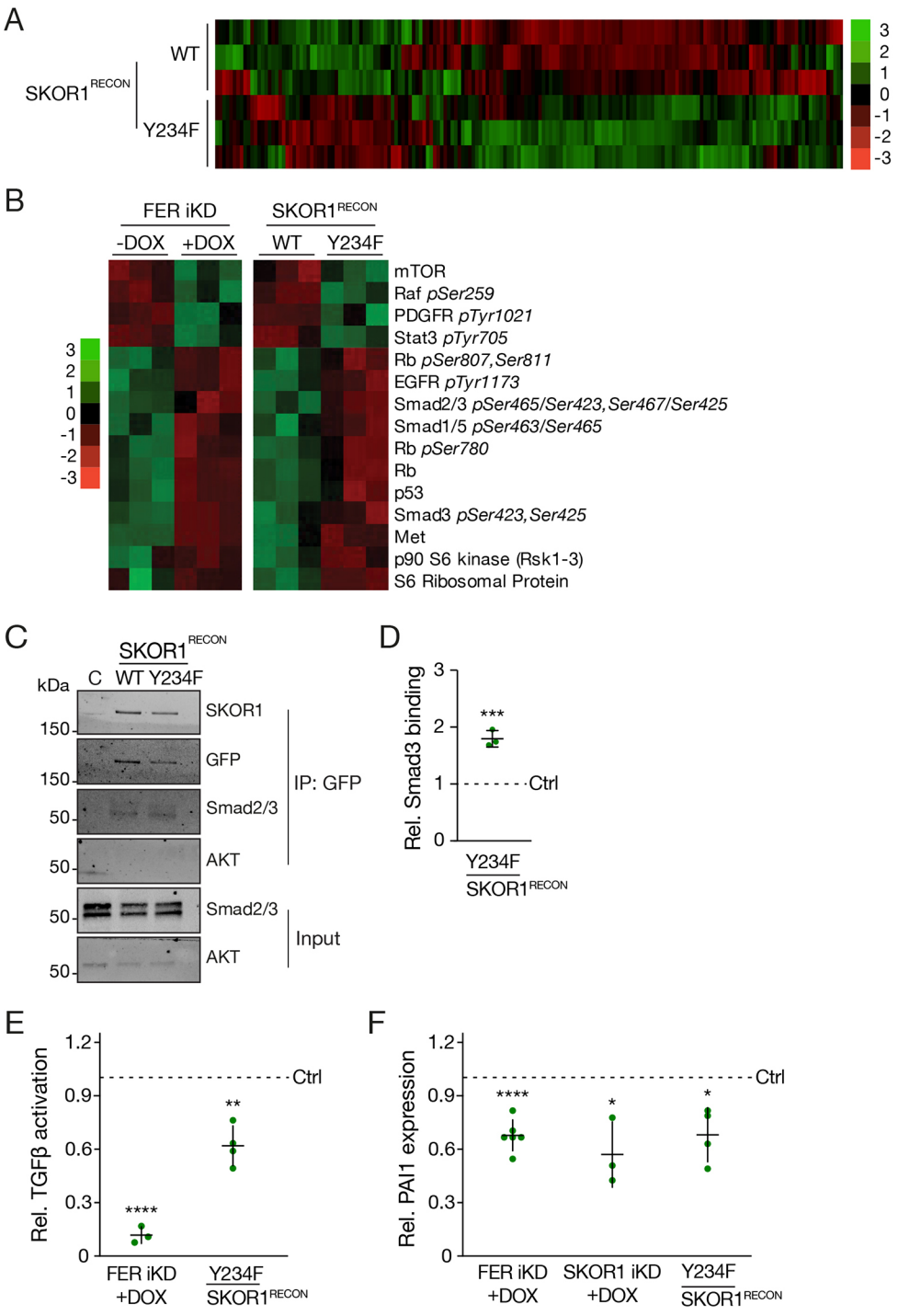

Fig. 5. FER and SKOR1 Y234 promote Smad2/3 phosphorylation. (A,B) SKOR1 Y234 controls multiple key signaling pathways in MM231 cells (A). FER and SKOR1 Y234 similarly induce phosphorylation of Smad2/3 and other key growth signaling effectors (B). Heatmaps representing altered levels of phosphorylated protein residues (Z-scores) are shown. Rows represent phosphorylation sites and colors represent magnitude of intensity. The red-to-green scale indicates signal intensity. (C,D) The SKOR1 Y234 residue controls SKOR1 binding to Smad3. Smad2/3 binding to SKOR1 was assessed in MM231 $SKOR1^{RECON}$ cells using co-immunoprecipitation (IP) for GFP and western blotting. Cell lysates from parental MM231 cells were used as non-specific IP controls. Shown are the protein levels of Smad2/3 and SKOR1. AKT was used as a loading control. Fold changes of Smad2/3 levels bound to GFP-$SKOR1^{WT}$ and GFP-$SKOR1^{Y234F}$ were quantified relative to control input samples (shown as a dashed line) in D. (E,F) Phosphorylation of SKOR1 Y234 regulates Smad3-specific activation of TGFβ-induced transcription. Relative fold change of TGFβ/Smad3 activation was determined upon FER depletion and $SKOR1^{Y234F}$ reconstitution (E) in MM231 cells transfected with the TGFβ/Smad3-inducible $CAGA_{12}$ luciferase transcriptional reporter construct. SKOR1 and FER regulate mRNA expression of *PAI1*, a TGFβ target gene. Relative *PAI1* expression was determined upon FER depletion, SKOR1 depletion and $SKOR1^{Y234F}$ reconstitution (F) in MM231 cells. Relative fold changes in E,F were quantified relative to control samples (Ctrl, dashed lines). Quantifications are from at least three independent experiments. Expression was normalized by *GAPDH*. Error bars denote s.d. **P*<0.05; ***P*<0.01; ****P*<0.001; *****P*<0.0001; unpaired two-tailed *t*-test.

Smad signaling, we assessed SKOR1 binding to Smad. For this, we performed co-immunoprecipitation assays in $SKOR1^{RECON}$ cells, which confirmed that $SKOR1^{WT}$ precipitated with Smad2 and Smad3, and we noted a higher affinity to Smad3 (Fig. 5C, lower band). $SKOR1^{Y234F}$ reconstitution increased binding to Smad3 compared to $SKOR1^{WT}$ (Fig. 5C; quantified in Fig. 5D), suggesting that phosphorylation of Y234 in SKOR1 weakens binding to Smad3. Because Smad3-dependent transcriptional activation downstream of the TGFβ/Smad signaling pathway depends on Smad3 translocation to the nucleus, we applied the $CAGA_{12}$-luciferase transcriptional reporter as an indirect readout of nuclear Smad3 activation (Dennler et al., 1998). Either FER depletion or SKOR1 reconstitution with the Y234F mutant (Fig. 5E) led to a significant decrease of Smad3-dependent transcriptional activity. To further assess whether FER and SKOR1 impact Smad3-dependent signaling pathways, we assessed the mRNA levels of plasminogen activator inhibitor 1 (PAI1, also known as SERPINE1), a Smad3 effector that is specifically upregulated in Smad3-driven tumor progression (Petersen et al., 2010). Either FER or SKOR1 loss led to a decrease in *PAI1* mRNA expression in MM231 cells (Fig. 5F). We also observed that *PAI1* expression was significantly decreased upon $SKOR1^{Y234F}$ reconstitution (Fig. 5F). Taken together, these data suggest that FER-dependent phosphorylation of SKOR1 on Y234 might regulate binding of

Journal of Cell Science

Journal of Cell Science (2023) 136, jcs260243. doi:10.1242/jcs.260243

SKOR1 to Smad3, thereby facilitating phosphorylation and activation of Smad3-dependent signals.

SKOR1 promotes tumor growth and metastasis in mouse xenografts

We next orthotopically transplanted luciferase-expressing MM231 SKOR1 iKD cells in recipient female mice and measured primary tumor growth and metastasis development over time. As SKOR1 loss inhibited proliferation in MM231 cells, we transplanted untreated cells, monitored animals until palpable tumors (~50 mm^3) formed in both groups and started DOX administration to induce SKOR1 knockdown. Real-time quantitative PCR (qPCR) was used to quantify *SKOR1* mRNA in tumor samples, which confirmed our *in vitro* data that SKOR1 expression is downregulated to approximately 50% after knockdown compared with controls (Fig. 6A). In contrast to FER kinase inhibition, SKOR1 loss significantly affected primary tumor growth (Fig. 6B). Moreover, bioluminescence imaging showed that SKOR1 loss impaired the development of lung metastases, leading to increased metastasis-free survival (Fig. 6C,D). In contrast to control tumors, SKOR1-depleted tumors tended to show expansive growth patterns with little to no invasion into the stroma and adjacent muscle layers of the mammary fat pad (Fig. 6E). From these results, we conclude that SKOR1 promotes tumor growth and metastasis of high-grade and basal-like breast cancer cells in mice, suggesting that SKOR1 contributes to tumor progression in breast cancer.

DISCUSSION

Because SKOR1 expression has been predominantly observed in brain tissues, most studies have focused on its role during neuronal development (Arndt et al., 2007). Now, our study identifies SKOR1 as a direct FER substrate *in vitro* and an important regulator of breast cancer growth and metastasis formation *in vivo*. We propose that SKOR1 plays a key role in promoting cell proliferation and migration, thereby driving tumor progression and metastasis formation. Interestingly, SKOR1 expression has been associated with migration of other cell types. SKOR1 is expressed in Purkinje cells throughout all stages of embryonic development and in adulthood, with particularly high levels noted in the migratory precursors of Purkinje cells (Arndt et al., 2007). In the early stages of wound healing, SKOR1 expression is upregulated in fibroblasts, in which it might control cellular migration by affecting F-actin dynamics and/or organization (Arndt et al., 2011). Elevated SKOR1 levels are sustained in fibro-proliferative diseases, including keloid scars and skin sclerosis (Arndt et al., 2011), possibly contributing to the pathogenesis of these diseases by promoting the migration of dermal fibroblasts into the wound site, reorganizing the collagen structure that is deposited by these fibroblasts, and controlling collagen contraction (Arndt et al., 2011). In line with our data showing that SKOR1 loss induces stress fiber and FA formation and impairs migration, overexpression of SKOR1 in fibroblasts promotes cell motility by driving F-actin and FA complex redistribution at the cell periphery (Arndt et al., 2011). Based on these observations and our findings, SKOR1 appears to play a critical role in regulating cytoskeletal organization to control cell morphology and promote cell motility (Arndt et al., 2011).

Here, we propose that SKOR1 acts downstream of FER, because SKOR1 loss-of-function phenotypes are nearly identical to FER kinase inactivation (Ivanova et al., 2013; Sangrar et al., 2007). Although the kinase activity of FER appears to only modestly contribute to the proliferation of MM231 cells, SKOR1 loss of function profoundly impacts cellular growth. Although we have no clear hypothesis or data explaining the mechanism that controls the inhibition of proliferation upon SKOR1 knockdown, we also cannot exclude the possibility that phosphorylation of SKOR1 on Y234 by FER induces pro-proliferative cues stemming from SKOR1.

In previous studies, we determined that FER regulates actin dynamics and FA distribution via endosomal recycling of growth factor receptors and cell adhesion molecules, and that dysregulation of membrane trafficking upon FER depletion greatly impairs the migratory and invasive behavior of breast cancer cells (Ivanova et al., 2013; Tavares et al., 2022). Because SKOR1 belongs to a well-known family of major regulators of TGFβ signaling, a pathway for which endosomal recycling of TGFβ receptors is essential (Yakymovych et al., 2017), we decided to examine whether SKOR1 promotes FER-dependent cytoskeletal organization and invasion in TNBC through TGFβ signaling. In early endosomes, signaling-promoting factors, such as Smad anchor for receptor activation (SARA), support Smad2/3 and TGFβ receptor interaction, which facilitate TGFβ signaling and downstream Smad2/3 phosphorylation (Chen, 2009; Nawshad et al., 2005). Phosphorylated Smad2/3 forms a heterotrimeric complex with Smad4 that translocates to the nucleus, where it associates with transcription factors and coregulators to control expression of >500 specific target genes (Tecalco-Cruz et al., 2018). Interestingly, our results show that loss of FER expression and $SKOR1^{Y234F}$ similarly affects the phosphorylation levels of several growth factor receptors and downstream signaling factors, including decreased phosphorylation of the TGFβ signaling mediator Smad2/3. Similar to SARA, Ski, SnoN and SKOR2 are Smad-interacting proteins that regulate TGFβ signaling through simultaneous interaction with Smad proteins (Tecalco-Cruz et al., 2018; Wu et al., 2002). Interestingly, we find that SKOR1 preferentially binds to Smad3 in TNBC cells, an observation that agrees with previous reports (Arndt et al., 2007; Takaesu et al., 2012). Although Ski and SnoN proteins mainly localize to the nucleus to bind Smad4 and act as transcriptional corepressors through the I-loop of their SAND domain (Nicol et al., 1999; Nicol and Stavnezer, 1998), SKOR1 shows a predominant cytoplasmic and vesicular-like localization in MM231 cells, suggesting control over Smad3 in the cytosol. Our data indicate that FER phosphorylates SKOR1 on Y234, a residue located in the I-loop of SKOR1 (Arndt et al., 2007), and that the loss-of-function Y234F mutation increases Smad3 binding to SKOR1. These results suggest that FER-dependent SKOR1 phosphorylation promotes dissociation of SKOR1–Smad2/3 complexes and thereby potentiates TGFβ signaling through a release of Smad2/3 molecules and subsequent recruitment by signaling-promoting factors, such as SARA (Fig. 6F). Furthermore, we suggest that potentiation of TGFβ signaling through releasing Smad3 upon phosphorylation of SKOR1 Y234 by FER leads to transcriptional expression of *PAI1*, a known player in cancer progression (Petersen et al., 2010). *PAI1* expression is known to induce tumor angiogenesis (Isogai et al., 2001) and promotes breast cancer cell migration through the induction of F-actin-dependent formation of membrane protrusions (Chazaud et al., 2002; Liu et al., 2020). Hence, although the exact mechanism by which SKOR1 regulates FA distribution and actin dynamics is still unclear, these studies suggest that SKOR1 activity can induce cytoskeletal organization and promote cell migration, possibly through Smad3 signaling and *PAI1* expression. It has also been reported that Smad3 can upregulate the expression of ubiquitin ligases that target RhoA for degradation (Yu et al., 2015). Activation of RhoA is essential for FA assembly and stress fiber formation (Aguilar-Rojas et al., 2012).

Journal of Cell Science (2023) 136, jcs260243. doi:10.1242/jcs.260243

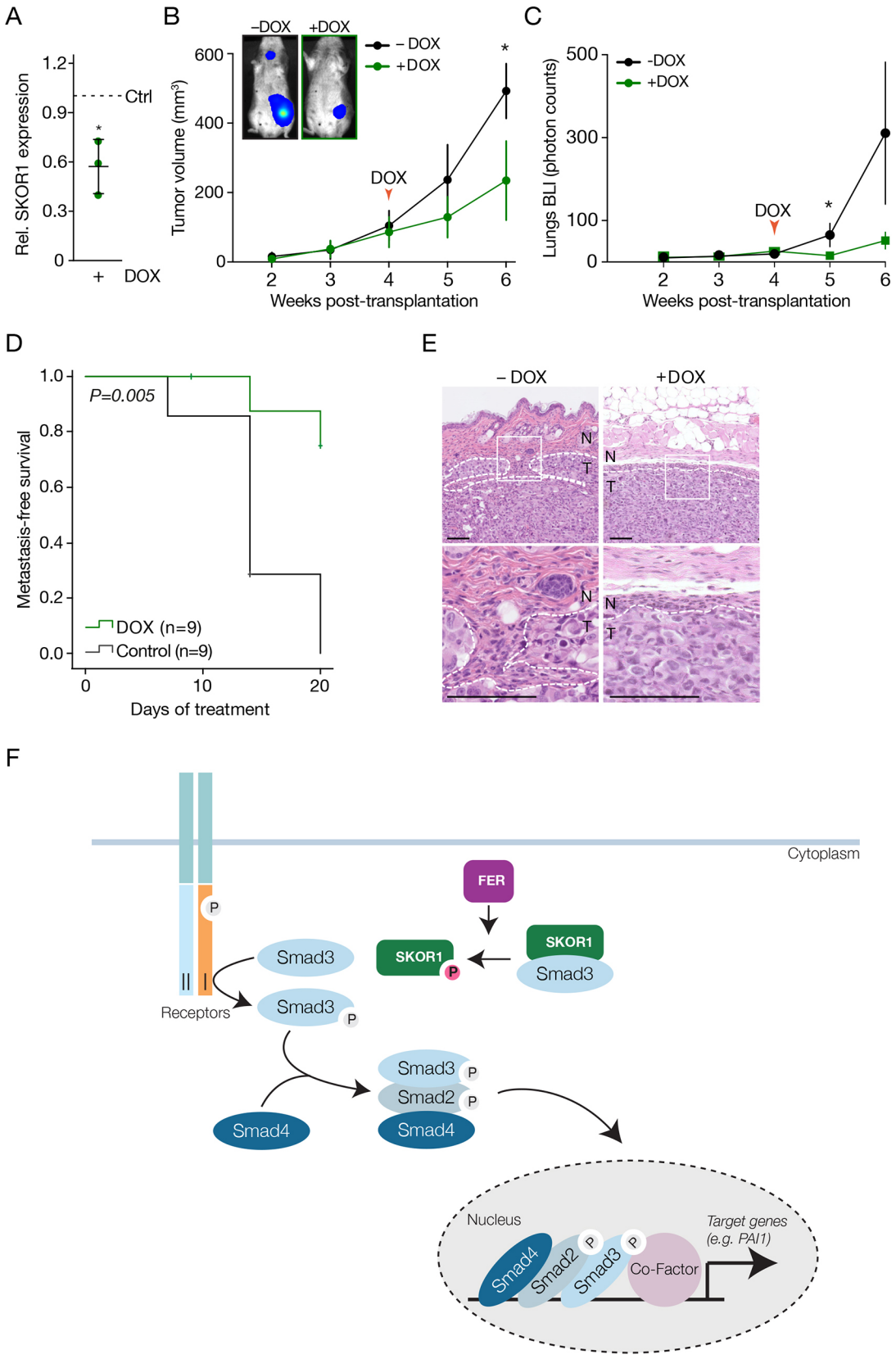

Fig. 6. See next page for legend.

Because we observed these features in SKOR1-depleted and SKOR1^{Y234F}-expressing cells, it suggests that SKOR1 loss or SKOR1^{Y234F} expression might cause sustained RhoA activity by decreasing Smad3 signaling, thereby inducing F-actin bundling and FA formation. Conversely, SKOR1 Y234 phosphorylation by FER could promote Smad3-dependent degradation of RhoA, leading to

Journal of Cell Science (2023) 136, jcs260243. doi:10.1242/jcs.260243

Fig. 6. SKOR1 promotes breast tumor growth and metastasis formation. (A) Validation of SKOR1 knockdown in mice breast tumors. Fold change of SKOR1 expression relative to control samples (Ctrl, dashed line) by real-time qPCR. (B–D) SKOR1 promotes breast tumor growth and metastasis formation in mice. Luciferase-expressing MM231 SKOR1 iKD cells were xenografted and switched to a DOX-containing diet (red arrow) upon formation of palpable tumors. Primary tumor volume (B) and lung metastasis formation (C) were monitored weekly. Kaplan–Meijer analysis was used to determine cumulative survival of mice treated with (*n*=9) or without (*n*=9) DOX (D). Error bars denote s.d. **P*<0.05; unpaired two-tailed *t*-test. BLI, bioluminescence imaging. (E) SKOR1 promotes tumor invasion in mice. Representative Haematoxylin and Eosin-stained images of mice treated or untreated with DOX at end points. Dashed white lines indicate the tumor (T)–normal (N) breast tissue border. Inset images correspond to a 200% magnification. Scale bars: 100 µm. (F) Schematic model depicting SKOR1 as a mediator of FER-dependent Smad2/3 signaling pathways.

F-actin redistribution and disassembly of FAs to increase cell migration and invasion.

In closing, we present evidence that SKOR1 mediates FER-dependent tumor cell migration and invasion in breast cancer cells through the regulation of actin cytoskeleton dynamics and FA formation. Our data show that the SKOR1 Y234 residue, a candidate FER kinase phosphorylation site, is critical for the invasive growth of basal-type breast cancer cells. Although further studies will be needed to provide formal proof for phosphorylation of SKOR1 Y234 *in vivo*, our work substantiates FER as a cardinal tumor progression factor and advocates inhibition of FER kinase activity as a promising intervention for high-grade and basal-type breast cancers.

MATERIALS AND METHODS

Constructs, virus generation and transduction

SKOR1 exon 5 WT and Y^{NULL}, in which all tyrosine residues were substituted by alanine residues, were ordered as gene blocks, subcloned in the pJET1.2/blunt cloning vector (Fermentas by Thermo Fisher Scientific, St. Leon-Rot, Germany) and inserted into the NotI/EcoRI sites of pGEX-6P-1 (GE Healthcare, 28-9546-48) to introduce the GST tag. For stable knockdown (KD) of *SKOR1*, human *SKOR1* shRNA pLKO.1-puro constructs (#1, 5′-CGAGCCAGATAAGGAAGACAA-3′; #2, 5′-CCT-ATCCAGACCAAAGGAGTA-3′) were used. pLKO.1-TRC (shSCR) (Addgene, 10879) was used as a control. The inducible SKOR1 RNAi system was generated as described previously using the shSKOR1 #1 sequence (Schackmann et al., 2011). To generate GFP–SKOR1-expressing constructs, full-length *SKOR1* cDNA was obtained from transOMIC (BioCat, gene ID 390598) and was cloned into a Gateway-compatible entry vector (Thermo Fisher scientific) (pENTR-SKOR1), and subsequently recombined into destination vectors using the Gateway LR Clonase II Enzyme Mix (Invitrogen, 11791-020, Carlsbad, CA). Mutations were introduced in pENTR-SKOR1 following the QuikChange II XL Site-Directed Mutagenesis protocol (Agilent Technologies, Wilmington, DE). Three silent mutations (indicated in bold and underlined) were introduced to create resistance to sh901 (SKOR1-shRes) using the primers 5′-GAA-ACGAGGAAATCCTA**C**CCAGACCAAAG**A**AG**C**ATCTCCCAGCC-3′ (forward) and 5′-GGCTGGGAGAT**G**CT**T**CTTTGGTCTGG**G**TAGG-ATTTCCTCGTTTC-3′ (reverse). The Y234F mutation was introduced using the primers 5′-CCGACGCCAAGTTCACGCAGCCCGA-3′ (forward) and 5′- TCGGGCTGCGTGAACTTGGCGTCGG-3′ (reverse), generating pENTR-SKOR1-shRes-Y234F. SKOR1-shRes-WT and SKOR1-shRes-Y234F were then recombined into pLenti CMV-GFP (658-5) (Addgene, 17448). For transduction of the above-mentioned constructs, pLV-PGK-GFP (Addgene, 19070) was included as a control. Lentiviruses were produced in HEK239T cells, followed by cell transduction as described previously (Schackmann et al., 2011) and 1 week of puromycin selection (2 µg/ml) to obtain stable SKOR1 KD MM231 cells. For CRISPR-based gene editing, oligonucleotides encoding single guide RNA (gRNA) sequences targeting FER (sense, 5′-AAATCCTTGGAGACTTTACG-3′, and anti-sense, 5′-CGTAAAGTCTCCAAGGATTT-3′) were annealed by heating to 95°C, followed by a gradual cooldown to room temperature. Annealed oligonucleotides were ligated into BbsI-digested pACEBac1-Cas9-GFP (kind gift from Susanne Lens, University Medical Center Utrecht, The Netherlands; Hindriksen et al., 2017). Left and right homology arms (LHA and RHA, respectively) were designed according to the In-Fusion cloning strategy and ordered as gene blocks (Fig. S1A). Each homology arm was subcloned into the pJET1.2/blunt cloning vector and inserted into pUNKI-puro (kindly provided by Susanne Lens). LHA was first ligated into the ClaI/AscI sites of pUNKI, followed by ligation of RHA into the SacI/SalI sites to generate pUNKI-puro-LHA-RHA. The puro-LHA-RHA cassette was then inserted into the gRNA-containing pACEBac1-Cas9-GFP by NotI restriction cloning, generating pACEBac1_FER-AS. All constructs were verified by Sanger DNA sequencing.

Cell culture and transfection

MDA-MB-231 (MM231) cells were obtained from Cell Lines Service (Eppelheim, Germany) and SUM149PT were obtained from Asterand (Detroit, MI). Both were STR verified and grown in Dulbecco's modified Eagle medium (DMEM; Invitrogen, 11039-047, Carlsbad, CA), supplemented with 1% penicillin-streptomycin (Invitrogen, 15070-063) and 10% fetal bovine serum (FBS) (Invitrogen, 16050-122). Cells were cultured at 37°C with 5% CO_2. MM231 FER iKD cells have been generated previously (Ivanova et al., 2013). MM231 cells were transfected with pACEBac1_FER-AS using FuGene HD (Promega, E2311) according to the manufacturer's instructions. Two days after transfection, cells were treated with 2 µg/ml puromycin for 1 week, followed by single-cell expansion. Positive FER^{ASKI} clones were selected by PCR and sequencing with the primers 5′-TGAGGGAAGGCTTTACTCGTT-3′ (forward) and 5′-TC-CTTGGAGACTTTACGAGGAG-3′ (reverse). MM231 FER^{ASKI} cells and MM231 parental cells were treated with 1 µM NM-PP1 (Calbiochem) for 3 days. DOX-inducible cell lines were treated for 5 days with 2 µg/ml doxycycline (Sigma-Aldrich, D9891-1G), refreshed on day 3.

For 3D assays, MM231 cells were added to Cultrex Basement Membrane Extract (BME; Trevigen, 3533-005-02) at a density of 500 cells/100 µl BME. Droplets of 25 µl were added to flat-bottomed, optical plastic 24-well plates (Corning, Tewksbury, MA). Plates were incubated for 45 min at 37°C to allow the BME to solidify, after which 500 µl normal growth medium was added. Cells were cultured for 7 days at 37°C.

3D morphology assessment

Bright-field images were acquired by using a 10× objective on an EVOS M5000 Imaging System (Thermo Fisher Scientific). At least five images were acquired per chamber well, and at least two wells were imaged per condition. Each image was segmented by individually optimizing the OrganoSeg (Borten et al., 2018) parameters manually until a suitable segmentation was achieved. Invasiveness was inferred using the 'solidity' parameter (invasiveness=1−solidity) reported in each spheroid caption.

Expression of recombinant proteins and *in vitro* kinase assays

Protein expression in the *Escherichia coli* strain Rosetta was induced by incubation with 0.2 mM isopropyl β-D-1-thiogalactopyranoside (IPTG) for 16 h at 18°C. Recombinant proteins were extracted from bacterial pellets by adding lysis buffer (10 mM EGTA, 10 mM EDTA, 0.1% Tween 20, 250 mM NaCl, 5 mM dithiothreitol) supplemented with 0.325 mg/ml lysozyme and a cocktail of protease inhibitors (Complete EDTA-free, Roche, Basel, Switzerland). Samples were sonicated, centrifuged and coupled to glutathione-sepharose 4B beads (Amersham Biosciences), followed by elution with elution buffer (100 mM Tris pH 8.0, 30 mM glutathione and 75 mM KCl). Eluates were treated with sample buffer (375 mM Tris-HCl pH 6.8, 25% glycerol, 12.5% β-mercaptoethanol, 10% SDS, 0.025% bromophenol blue) and boiled. Proteins were separated on 15% SDS-PAGE gels and stained with Instant Blue (Abcam, ab119211).

Recombinant analogue-sensitive (AS) or kinase-dead (D742R) GST–FER was incubated with WT or Y^{NULL} exon 5 GST–SKOR1, or GST–cortactin as substrate. Each reaction was performed in 25 µl kinase buffer (10 mM $MnCl_2$, 20 mM Tris-HCl pH 7.5, 0.1 mM sodium orthovanadate) supplemented with

Journal of Cell Science (2023) 136, jcs260243. doi:10.1242/jcs.260243

250 µM N-benzyl (Bn)-ATPγS (B 072-05, BioLog), with or without 10 µM NM-PP1 (Merck). After 30 min incubation at 30°C, reactions were terminated by the addition of 2.5 mM EDTA and subsequently incubated with 2.5 mM p-nitrobenzyl mesylate (Epitomics, Burlingame, CA) for 2 h at room temperature. The reactions were stopped by adding sample buffer. The bio-orthogonal thiophosphate ester generated by the p-nitrobenzyl mesylate was recognized by a thiophosphate ester-specific antibody.

Immunoblotting

Proteins were extracted from cells by scraping in sample buffer and lysed for 10 min on ice, followed by 10 min of boiling. Protein extracts and *in vitro* kinase reaction products were separated by SDS-PAGE and blotted onto PDVF membranes. Following 1 h blocking with 5% bovine serum albumin (BSA) in TBS containing 0.1% Tween 20 (TBST), the membrane was incubated with primary antibodies in blocking buffer overnight at 4°C. After washing three times with PBS containing 0.1% Tween 20, the membranes were probed with either horseradish peroxidase-conjugated secondary antibodies (DAKO, 1:10,000) or IRDye 680- and 800-conjugated secondary antibodies (LI-COR, 1:5000) for 1 h at room temperature and visualized using Enhanced Chemo-Luminescence (ECL; GE Healthcare) or Typhoon Biomolecular Imager (GE Healthcare), respectively. The following primary antibodies and dilutions were used for western blotting: rabbit anti-phospho-Src (Invitrogen, 44-660G, 1:1000), rabbit anti-GAPDH (Sigma-Aldrich, G9545, 1:1000), mouse anti-GAPDH (Millipore, Mab374, 1:1000), rabbit anti-thiophosphate ester (Abcam, ab92570, 1:5000), mouse anti-GST (Santa Cruz Biotechnology, sc-138, 1:1000), mouse anti-GFP (Santa Cruz Biotechnology, sc-8334, 1:500), rat anti-GFP (3HG) (Chromotek, 029762, 1:1000), goat anti-AKT (Santa Cruz Biotechnology, sc-1618, 1:1000), mouse anti-pY20 (BD Biosciences, 610011, 1:1000), rabbit anti-LBXCOR1 (Sigma-Aldrich, SAB2105374, 1:500), mouse anti-Smad2/3 (C-8) (Santa Cruz Biotechnology, sc-133098, 1:1000) and rabbit anti-phospho-EGFR Y1173 (Cell Signaling Technology, 4407, 1:500). The images of uncropped western blots are shown in Fig. S7.

3D invasion assay, BrdU incorporation and immunofluorescence

Invasion and proliferation were assessed by incubating cells in BME (3D) with 10 µm BrdU for 2 h. Cells were fixed with 4% paraformaldehyde and 1% glutaraldehyde (Sigma-Aldrich, G5882), followed by 1% $NaBH_4$ treatment for 30 min. Then, cells were washed with PBS before 2 M HCl treatment for 80 min. Fixed cultures (3D) were blocked overnight in 5% goat serum and 0.3% Triton X-100 in PBS, followed by incubation with 10 µl/ml Alexa Fluor 647-conjugated anti-BrdU antibody (BD Biosciences, 560209) or anti-cleaved Caspase 3 (Cell Signaling Technology, 9661s, 1:250) in 1% BSA and 0.3% Triton X-100 in PBS overnight. The structures were washed three times and then probed with secondary antibodies (when applicable), Alexa Fluor 568-conjugated phalloidin (Thermo Fisher Scientific, A12380, 1:200) and DAPI in 1% BSA and 0.3% Triton X-100 in PBS overnight.

For 2D assays, cells were grown on 12 mm coverslips and fixed for 30 min using 4% paraformaldehyde. Fixed cells were permeabilized with 0.1% Triton X-100 in PBS for 3 min, blocked with 5% BSA for 30 min and incubated with primary antibodies in 1% BSA in PBS overnight at 4°C. Cells were washed three times and then probed with secondary antibodies and Alexa Fluor 568-conjugated phalloidin (1:200) in 1% BSA for 2 h. After three washes in PBS, cells were stained with 2 µg/ml DAPI (Sigma-Aldrich, D9542) in 1% BSA for 5 min. Again, cells were washed thrice with PBS before mounting using ProLong Diamond Antifade (Invitrogen). The primary antibody used was rabbit anti-phospho-Paxillin (pPax; Life Technologies, 447226, 1:200). The secondary antibody used was goat anti-rabbit Alexa Fluor 647 (Molecular Probes by Invitrogen, A32733, 1:200).

An inverted Carl Zeiss LSM 700 Laser Scanning Microscope with a Plan-Apochromat 63×/1.40 oil DIC M27 or with a LD Plan-Neofluar 40×/0.6 Korr M27 objective was used for imaging. Confocal images were analyzed using ImageJ Software.

Co-immunoprecipitation

GFP-tagged proteins were immunoprecipitated using a GFP-trap system (ChromoTek, gta-10) as described previously (van de Ven et al., 2015). After washing with lysis buffer, bound and non-bound proteins were eluted in sample buffer, boiled and analyzed by western blotting.

Cell migration assay

The migratory abilities of MM231 overexpressing $SKOR1^{WT}$ or $SKOR1^{Y234F}$, MM231 SKOR1 iKD, SUM149PT SKOR1 iKD and MM231 FER^{ASKI} cells were assessed using live-cell imaging. MM231 SKOR1 iKD and SUM149PT SKOR1 iKD cells were induced for 5 days with or without DOX. MM231 FER^{ASKI} cells were treated for 3 days with NM-PP1 or DMSO (control), before plating them on 24-well plastic-bottomed plates (Corning). MM231 SKOR1 iKD and $SKOR1^{RECON}$ cells were incubated with 200 nM SiR-DNA (Spirochrome) for 7–8 h before imaging. SUM149PT SKOR1 iKD and MM231 cells expressing $SKOR1^{WT}$ or $SKOR1^{Y234F}$ were incubated with 1 µg/ml Hoechst for 10 min. Cells were imaged every 10 min for 16 h using a Carl Zeiss Cell Observer widefield microscope with an EC Plan-Neofluar 5×/0.16 M27 objective. During imaging, cells were kept in complete DMEM medium (with or without DOX, or with DMSO or NM-PP1) under normal growth conditions (37°C, 5% CO_2). Cell migration was quantified using the Imaris for Tracking software (Bitplane, Oxford Instruments, UK) or TrackMate (Tinevez et al., 2017) plugin.

Real-time quantitative PCR

Total RNA from the samples was extracted using the RNeasy Plus Mini Kit (QIAGEN, 74104) following the manufacturer's guidelines. cDNA synthesis was performed using the iScript cDNA Synthesis Kit (Bio-Rad). qPCR reactions were performed using FastStart Universal SYBR Green Master Mix (Roche, 4913957001) and the CFX96 touch Real-Time PCR detection system (Bio-Rad). mRNA levels were normalized to their corresponding *GAPDH* expression levels. Knockdown efficiency was quantified using the Pfaffl method (Pfaffl, 2001). The following oligonucleotide primer pairs were used: SKOR1 forward, 5′-CCACGAGCCAGATAAGGAAG-3′, and SKOR1 reverse, 5′-CCATTT-GTTCCAGGAGCAGT-3′; PAI1 forward, 5′-TCTTTGGTGAAGGGTC-TGCT-3′, and PAI1 reverse 5′-CTGGGTTTCTCCTCCTGTTG-3′; and GAPDH forward, 5′- TGCACCACCAACTGCTTAGC-3′, and GAPDH reverse, 5′-GGCATGGACTGTGGTCATGAG-3′.

Colony formation assays

MM231 SKOR1 iKD cells were cultured with or without DOX for 5 days, and FER^{ASKI} cells were treated with DMSO or NM-PP1 for 3 days before seeding them at a density of 7500 cells into each well of a 24-well plate and culturing them for 3 days. Cells were fixed using 10% glutaraldehyde in normal growth medium for 10 min, stained using 0.1% Crystal Violet (Sigma-Aldrich) for 30 min while agitating, washed with water and dried overnight. 10% acetic acid (v/v) was used to elute the incorporated Crystal Violet for 30 min while agitating, after which the solution was quantified with a spectrophotometer at 590 nm (Bio-Rad).

RPPA

MM231 SKOR1 iKD cells were cultured with or without DOX for 5 days, and FER^{ASKI} cells were treated with DMSO or NM-PP1 for 3 days. Cell extracts were prepared in RIPA [50 mM Tris-HCl pH 7.4, 150 mM NaCl, 1 mM EDTA pH 8.0, 1 mM EGTA, 1% Triton X-100, 0.1% SDS, 10 mM glycerol phosphate, protease inhibitor cocktail (Complete, Sigma-Aldrich) and phosphatase inhibitor (Roche, phosSTOP)]. RPPA was performed as described previously (Teo et al., 2018). Briefly, samples were adjusted to 1 mg/ml then serially diluted and spotted in triplicate onto single pad Avid Nitrocellulose slides (Grace Biolabs) using an Aushon 1740 Arrayer platform with 185 µm pins. Slides were washed for 4× 15 min in deionised water and antigen retrieval was carried out by incubating with 1× Reblot strong for 15 min. Slides were then washed for 2× 5 min in deionised water, then 2×5 min with PBS with 0.1% Tween 20 and incubated for 10 min with block buffer (Superblock T20 in TBS; Pierce/Thermo Fisher Scientific #37536). Slides were incubated with primary antibodies diluted 1:250 in Superblock T20 for 1 h. Slides were then washed in TBST for 2× 5 min, blocked for 10 min, washed 3× 5 min with TBST and incubated with

secondary antibodies (Dylight-800-labeled anti-species antibodies, Thermo Scientific) diluted 1:2500 in Superblock T20 for 30 min. Slides were then washed 2× 5 min in TBST, rinsed in deionised water and dried. Slides were scanned using an Innopsys 710 slide scanner and images analysed using Mapix software (Innopsys), with average signal intensity with background intensity subtracted determined for each spot.

Smad3/Smad4-dependent $CAGA_{12}$-luciferase transcriptional reporter assays

MMM231 FER iKD were treated with or without DOX for 5 days. $SKOR1^{RECON}$ $SKOR1^{WT}$ and $SKOR1^{RECON}$ $SKOR1^{Y234F}$ cells were treated with DOX for 5 days. Then, ∼50,000 cells were plated in 6-well plates and transiently transfected with 0.4 µg of the TGFβ/Smad3-inducible $CAGA_{12}$ luciferase transcriptional reporter construct (Dennler et al., 1998) and 1.44 µg of the internal control pRL-TK vector (Peter ten Dijke, LUMC), using Lipofectamine 2000 (Alfagene, 11668-019) according to the manufacturer's instructions. Cells were serum starved for 8 h before stimulation with 7 ng/ml of human recombinant TGFβ1 (Invitrogen, PHG9204) and luciferase activities were quantified 24 h later using the Dual Luciferase Assay (Promega, PROME19600010). Briefly, 80 µl of lysed samples were added to 100 µl of luciferase assay reagent II in a 96-well plate. Firefly luminescence was detected using Synergy Mx (BioTek). Then, 100 µl of 1× Stop and Glo solution was added to detect Renilla luminescence. Each sample was evaluated in triplicate. Values were normalized with the Renilla luciferase activity expressed from the pRL-TK vector. Luciferase values shown in the figures are representative of transfection experiments performed in at least three independent experiments.

Mouse studies

Recipient female $RAG2^{-/-}$;$IL2R\gamma c^{-/-}$ immunodeficient mice (Envigo) were orthotopically transplanted (in the inguinal mammary gland) with luciferase-expressing MM231 cells (FER^{ASKI} or SKOR1 iKD) using a 50-µl Hamilton syringe (Hamilton, Bonadur, Switzerland). Mice were anesthetized using isoflurane (IsoFlo, Le Vet Pharma). Burprenorphine (0.1 mg/kg) was injected subcutaneously as analgesic treatment. After a recovery period of 2 weeks, mice were anesthetized with IsoFlo, injected intraperitoneally with 225 µg/g body weight of D-Luciferin firefly (L-8220 potassium salt; Biosynth) and imaged on a Biospace Φ bioluminescence imager (Biospace Lab). Tumor growth was measured using a digital pressure-sensitive caliper (Mitutoyo) on a weekly basis. Treatment started when tumors reached a volume of 50–100 mm^3. To study *in vivo* inactivation of FER, FER^{ASKI} mice were switched to water containing DMSO (solvent) or NM-PP1 (25 µM) *ad libitum*. Drinking water was refreshed twice a week. To deplete SKOR1 in cancer cells, SKOR1 iKD mice were switched from standard diet to DOX-containing chow (200 mg/kg; A155D70201; ssniff, Bio Services) *ad libitum*. Mice were euthanized if the mammary tumor reached a size of 1000mm^3, in the case of severe discomfort or when bioluminescence imaging revealed metastases.

Studies approval

All animal experiments were performed in accordance with local, national and European guidelines under the permit AVD115002015263 issued by the Netherlands Food and Consumer Product Safety Authority (NVWA) of the Ministry of Agriculture, Nature and Food Quality, the Netherlands.

Statistical analysis

Statistical analyses were performed using IBM SPSS Statistics (SPSS, Chicago, IL). The Kaplan–Meijer method was used for cumulative survival analysis; a two-way mixed-model ANOVA was used to evaluate differences in tumor volume. RPPA data were analyzed using an unpaired two-tailed *t*-test with multiple comparison testing using the Benjamini, Krieger and Yekutieli two-stage step-up method of correction in GraphPad Prism. Z-scores were calculated as (sample value – mean of antibody intensity across all samples)/standard deviation. Unbiased clustering was performed in Cluster 3.0 (Hoon et al., 2004) using Euclidean distance and average linkage, and heatmaps were made in Java TreeView (Saldanha, 2004). All other data were analyzed using one-way ANOVA with a Sidak post hoc test or unpaired two-tailed *t*-tests in GraphPad Prism 8.0. No statistical method was used to predetermine sample size. No samples were excluded from the analyses. All experiments were performed and quantified from at least three independent experiments (unless specified otherwise), and representative data are shown.

Online supplementary material

The online supplementary material shows how FER^{ASKI} cells were generated and validated. Fig. S2 shows that FER regulates key signaling pathways in MM231 breast cancer cells. Fig. S3 shows that FER regulates key signaling pathways in SUM149PT breast cancer cells. Fig. S4 shows that SKOR1 is necessary for the proliferation of MM231 breast cancer cells. Fig. S5 shows that SKOR1 is necessary for the migration of SUM149PT cells. Fig. S6 shows that overexpression of $SKOR^{WT}$ or $SKOR^{Y234F}$ impacts the migration of control MM231 cells. Fig. S7 shows the original blots that were cropped and shown in the other figures. We have also included the other replicates for experiments depicted in Fig. S1E and Fig. S5C. Table S1 lists significant RPPA substrates upon FER depletion in MM231 cells. Table S2 lists significant RPPA substrates upon FER depletion in SUM149PT cells. Table S3 lists significant RPPA substrates upon $SKOR1^{Y234F}$ reconstitution in MM231 cells.

Acknowledgements

We thank Peter ten Dijke for reagents and comments on the manuscript.

Competing interests

The authors declare no competing or financial interests.

Author contributions

Conceptualization: P.W.B.D., S.T.; Methodology: P.W.B.D., S.T.; Formal analysis: L.M.S., E.B., M.A.K.R., L.E., S.T.; Investigation: L.M.S., E.B., M.A.K.R., L.E., C.O.; Resources: M.H.; Writing - original draft preparation: L.M.S., S.T.; Writing - review & editing: L.M.S., V.G.B., P.W.B.D., S.T.; Supervision: P.W.B.D., S.T.; Funding acquisition: S.T., P.W.B.D.

Funding

This work was supported by KWF Kankerbestrijding (UU2014-7201), the Dutch Research Council (Nederlandse Organisatie voor Wetenschappelijk Onderzoek) TOP grant (NWO-TOP 02007) and the European Union's Horizon 2020 FET Proactive program under the grant agreement number 731957 (MECHANO-CONTROL).

Data availability

All relevant data can be found within the article and its supplementary information.

First Person

This article has an associated First Person interview with the first author of the paper.

Peer review history

The peer review history is available online at https://journals.biologists.com/jcs/article-lookup/doi/10.1242/jcs.260243.reviewer-comments.pdf

References

Aguilar-Rojas, A., Huerta-Reyes, M., Maya-Núñez, G., Arechavaleta-Velásco, F., Conn, P. M., Ulloa-Aguirre, A. and Valdés, J. (2012). Gonadotropin-releasing hormone receptor activates GTPase RhoA and inhibits cell invasion in the breast cancer cell line MDA-MB-231. *BMC Cancer* **12**, 550. doi:10.1186/1471-2407-12-550

Akiyoshi, S., Inoue, H., Hanai, J., Kusanagi, K., Nemoto, N., Miyazono, K. and Kawabata, M. (1999). c-Ski acts as a transcriptional co-repressor in transforming growth factor-β signaling through interaction with Smads. *J. Biol. Chem.* **274**, 35269-35277. doi:10.1074/jbc.274.49.35269

Allard, P., Zoubeidi, A., Nguyen, L. T., Tessier, S., Tanguay, S., Chevrette, M., Aprikian, A. and Chevalier, S. (2000). Links between Fer tyrosine kinase expression levels and prostate cell proliferation. *Mol. Cell. Endocrinol.* **159**, 63-77. doi:10.1016/S0303-7207(99)00205-1

Arndt, S., Poser, I., Moser, M. and Bosserhoff, A. K. (2007). Fussel-15, a novel Ski/Sno homolog protein, antagonizes BMP signaling. *Mol. Cell. Neurosci.* **34**, 603-611. doi:10.1016/j.mcn.2007.01.002

Arndt, S., Schmidt, J., Wacker, E., Karrer, S. and Bosserhoff, A.-K. (2011). Fussel-15, a new player in wound healing, is deregulated in keloid and localized scleroderma. *Am. J. Pathol.* **178**, 2622-2631. doi:10.1016/j.ajpath.2011.02.009

Arregui, C., Pathre, P., Lilien, J. and Balsamo, J. (2000). The nonreceptor tyrosine kinase fer mediates cross-talk between N-cadherin and beta1-integrins. *J. Cell Biol.* **149**, 1263-1274. doi:10.1083/jcb.149.6.1263

Aversa, C., Rossi, V., Geuna, E., Martinello, R., Milani, A., Redana, S., Valabrega, G., Aglietta, M. and Montemurro, F. (2014). Metastatic breast cancer subtypes and central nervous system metastases. *The Breast* **23**, 623-628. doi:10.1016/j.breast.2014.06.009

Bishop, A. C., Kung, C., Shah, K., Witucki, L., Shokat, K. M. and Liu, Y. (1999). Generation of Monospecific Nanomolar Tyrosine Kinase Inhibitors via a Chemical Genetic Approach. *J. Am. Chem. Soc.* **121**, 627-631. doi:10.1021/ja983267v

Bishop, A. C., Ubersax, J. A., Petsch, D. T., Matheos, D. P., Gray, N. S., Blethrow, J., Shimizu, E., Tsien, J. Z., Schultz, P. G., Rose, M. D. et al. (2000). A chemical switch for inhibitor-sensitive alleles of any protein kinase. *Nature* **407**, 395-401. doi:10.1038/35030148

Borten, M. A., Bajikar, S. S., Sasaki, N., Clevers, H. and Janes, K. A. (2018). Automated brightfield morphometry of 3D organoid populations by OrganoSeg. *Sci. Rep.* **8**, 5319. doi:10.1038/s41598-017-18815-8

Bottomley, M. J., Collard, M. W., Huggenvik, J. I., Liu, Z., Gibson, T. J. and Sattler, M. (2001). The SAND domain structure defines a novel DNA-binding fold in transcriptional regulation. *Nat. Struct. Biol.* **8**, 626-633. doi:10.1038/89675

Chazaud, B., Ricoux, R., Christov, C., Plonquet, A., Gherardi, R. K. and Barlovatz-Meimon, G. (2002). Promigratory effect of plasminogen activator inhibitor-1 on invasive breast cancer cell populations. *Am. J. Pathol.* **160**, 237-246. doi:10.1016/S0002-9440(10)64367-2

Chen, Y.-G. (2009). Endocytic regulation of TGF-β signaling. *Cell Res.* **19**, 58-70. doi:10.1038/cr.2008.315

Craig, A. W. and Greer, P. A. (2002). Fer kinase is required for sustained p38 kinase activation and maximal chemotaxis of activated mast cells. *Mol. Cell. Biol.* **22**, 6363-6374. doi:10.1128/MCB.22.18.6363-6374.2002

Dennler, S., Itoh, S., Vivien, D., Ten Dijke, P., Huet, S. and Gauthier, J. (1998). Direct binding of Smad3 and Smad4 to critical TGFβ–inducible elements in the promoter of human plasminogen activator inhibitor–type 1 gene. *EMBO J.* **17**, 3091-3100. doi:10.1093/emboj/17.11.3091

Fischer, S., Bayersdorfer, F., Harant, E., Reng, R., Arndt, S., Bosserhoff, A.-K. and Schneuwly, S. (2012). fussel (fuss) - a negative regulator of BMP signaling in Drosophila melanogaster. *PLoS ONE* **7**, e42349. doi:10.1371/journal.pone.0042349

Gray, R., Bradley, R., Braybrooke, J., Liu, Z., Peto, R., Davies, L., Dodwell, D., Mcgale, P., Pan, H., Taylor, C. et al. (2019). Increasing the dose intensity of chemotherapy by more frequent administration or sequential scheduling: a patient-level meta-analysis of 37 298 women with early breast cancer in 26 randomised trials. *The Lancet* **393**, 1440-1452. doi:10.1016/S0140-6736(18)33137-4

Greer, P. (2002). Closing in on the biological functions of Fps/Fes and Fer. *Nat. Rev. Mol. Cell Biol.* **3**, 278-289. doi:10.1038/nrm783

Guo, C. and Stark, G. R. (2011). FER tyrosine kinase (FER) overexpression mediates resistance to quinacrine through EGF-dependent activation of NF-kappaB. *Proc. Natl. Acad. Sci. USA* **108**, 7968-7973. doi:10.1073/pnas.1105369108

Hindriksen, S., Bramer, A. J., Truong, M. A., Vromans, M. J. M., Post, J. B., Verlaan-Klink, I., Snippert, H. J., Lens, S. M. A. and Hadders, M. A. (2017). Baculoviral delivery of CRISPR/Cas9 facilitates efficient genome editing in human cells. *PLoS One* **12**, e0179514. doi:10.1371/journal.pone.0179514

Hoon, M. J . L., de, Imoto, S., Nolan, J. and Miyano, S. (2004). Open source clustering software. *Bioinformatics* **9**, 1453-1454. doi:10.1093/bioinformatics/bth078

Isogai, C., Laug, W. E., Shimada, H., Declerck, P. J., Stins, M. F., Durden, D. L., Erdreich-Epstein, A. and declerck, Y. A. (2001). Plasminogen activator inhibitor-1 promotes angiogenesis by stimulating endothelial cell migration toward fibronectin. *Cancer Res.* **61**, 5587-5594.

Ivanova, I. A., Vermeulen, J. F., Ercan, C., Houthuijzen, J. M., Saig, F. A., Vlug, E. J., Van Der Wall, E., Van Diest, P. J., Vooijs, M. and Derksen, P. W. B. (2013). FER kinase promotes breast cancer metastasis by regulating alpha6- and beta1-integrin-dependent cell adhesion and anoikis resistance. *Oncogene* **32**, 5582-5592. doi:10.1038/onc.2013.277

Ivanova, I. A., Arulanantham, S., Barr, K., Cepeda, M., Parkins, K. M., Hamilton, A. M., Johnston, D., Penuela, S., Hess, D., Ronald, J. et al. (2019). Targeting FER kinase inhibits melanoma growth and metastasis. *Cancers* **11**, 419. doi:10.3390/cancers11030419

Kapus, A., Ciano, C. D., Sun, J., Zhan, X., Kim, L., Wong, T. W. and Rotstein, O. D. (2000). Cell volume-dependent phosphorylation of proteins of the cortical cytoskeleton and cell-cell contact sites. The role of Fyn and FER kinases.. *J. Biol. Chem.* **275**, 32289-32298. doi:10.1074/jbc.M003172200

Kawakami, M., Morita, S., Sunohara, M., Amano, Y., Ishikawa, R., Watanabe, K., Hamano, E., Ohishi, N., Nakajima, J., Yatomi, Y. et al. (2013). FER overexpression is associated with poor postoperative prognosis and cancer-cell survival in non-small cell lung cancer. *Int J Clin Exp Pathol* **6**, 598-612.

Kennecke, H., Yerushalmi, R., Woods, R., Cheang, M. C. U., Voduc, D., Speers, C. H., Nielsen, T. O. and Gelmon, K. (2010). Metastatic behavior of breast cancer subtypes. *J. Clin. Oncol.* **28**, 3271-3277. doi:10.1200/JCO.2009.25.9820

Kim, L. and Wong, T. W. (1995). The cytoplasmic tyrosine kinase FER is associated with the catenin-like substrate pp120 and is activated by growth factors. *Mol. Cell. Biol.* **15**, 4553-4561. doi:10.1128/MCB.15.8.4553

Kim, L. and Wong, T. W. (1998). Growth factor-dependent phosphorylation of the actin-binding protein cortactin is mediated by the cytoplasmic tyrosine kinase FER. *J. Biol. Chem.* **273**, 23542-23548. doi:10.1074/jbc.273.36.23542

Kirsch, D. G. and Loeffler, J. S. (2005). Brain Metastases in Patients with Breast Cancer: New Horizons. *Clin. Breast Cancer* **6**, 115-124. doi:10.3816/CBC.2005.n.013

Ladwein, M. and Rottner, K. (2008). On the Rho'd: The regulation of membrane protrusions by Rho–GTPases. *FEBS Lett.* **582**, 2066-2074. doi:10.1016/j.febslet.2008.04.033

Li, H., Ren, Z., Kang, X., Zhang, L., Li, X., Wang, Y., Xue, T., Shen, Y. and Liu, Y. (2009). Identification of tyrosine-phosphorylated proteins associated with metastasis and functional analysis of FER in human hepatocellular carcinoma cells. *BMC Cancer* **9**, 366. doi:10.1186/1471-2407-9-366

Liu, J., Chen, Z., Huang, M., Tang, S., Wang, Q., Hu, P., Gupta, P., Ashby, C. R., Chen, Z.-S. and Zhang, L. (2020). Plasminogen activator inhibitor (PAI) trap3, an exocellular peptide inhibitor of PAI-1, attenuates the rearrangement of F-actin and migration of cancer cells. *Exp. Cell Res.* **391**, 111987. doi:10.1016/j.yexcr.2020.111987

Luo, K. (2004). Ski and SnoN: negative regulators of TGF-β signaling. *Curr. Opin. Genet. Dev.* **14**, 65-70. doi:10.1016/j.gde.2003.11.003

Luo, K., Stroschein, S. L., Wang, W., Chen, D., Martens, E., Zhou, S. and Zhou, Q. (1999). The Ski oncoprotein interacts with the Smad proteins to repress TGFβ signaling. *Genes Dev.* **13**, 2196-2206. doi:10.1101/gad.13.17.2196

Menges, C. W., Chen, Y., Mossman, B. T., Chernoff, J., Yeung, A. T. and Testa, J. R. (2010). A phosphotyrosine proteomic screen identifies multiple tyrosine kinase signaling pathways aberrantly activated in malignant mesothelioma. *Genes Cancer* **1**, 493-505. doi:10.1177/1947601910375273

Mizuhara, E., Nakatani, T., Minaki, Y., Sakamoto, Y. and Ono, Y. (2005). Corl1, a novel neuronal lineage-specific transcriptional corepressor for the homeodomain transcription Factor Lbx1*. *J. Biol. Chem.* **280**, 3645-3655. doi:10.1074/jbc.M411652200

Nawshad, A., Lagamba, D., Polad, A. and Hay, E. D. (2005). Transforming Growth Factor-β Signaling during Epithelial-Mesenchymal Transformation: Implications for Embryogenesis and Tumor Metastasis. *Cells Tissues Organs* **179**, 11-23. doi:10.1159/000084505

Nicol, R. and Stavnezer, E. (1998). Transcriptional Repression by v-Ski and c-Ski Mediated by a Specific DNA Binding Site*. *J. Biol. Chem.* **273**, 3588-3597. doi:10.1074/jbc.273.6.3588

Nicol, R., Zheng, G., Sutrave, P., Foster, D. N. and Stavnezer, E. (1999). Association of specific DNA binding and transcriptional repression with the transforming and myogenic activities of c-Ski. *Cell Growth Differ.*.**10**, 243-254.

Oshi, M., Okano, M., Maiti, A., Rashid, O. M., Saito, K., Kono, K., Matsuyama, R., Endo, I. and Takabe, K. (2020). Novel breast cancer brain metastasis patient-derived orthotopic xenograft model for preclinical studies. *Cancers* **12**, 444. doi:10.3390/cancers12020444

Pasder, O., Shpungin, S., Salem, Y., Makovsky, A., Vilchick, S., Michaeli, S., Malovani, H. and Nir, U. (2006). Downregulation of Fer induces PP1 activation and cell-cycle arrest in malignant cells. *Oncogene* **25**, 4194-4206. doi:10.1038/sj.onc.1209695

Petersen, M., Pardali, E., Van Der Horst, G., Cheung, H., Van Den Hoogen, C., Van Der Pluijm, G. and Ten Dijke, P. (2010). Smad2 and Smad3 have opposing roles in breast cancer bone metastasis by differentially affecting tumor angiogenesis. *Oncogene* **29**, 1351-1361. doi:10.1038/onc.2009.426

Pfaffl, M. W. (2001). A new mathematical model for relative quantification in real-time RT-PCR. *Nuc. Acids Res.* **29**, e45-e45. doi:10.1093/nar/29.9.e45

Rass, M., Gizler, L., Bayersdorfer, F., Irlbeck, C., Schramm, M. and Schneuwly, S. (2022). The Drosophila functional Smad suppressing element fuss, a homologue of the human Skor genes, retains pro-oncogenic properties of the Ski/Sno family. *PLoS ONE* **17**, e0262360. doi:10.1371/journal.pone.0262360

Ren, S. and Rollins, B. J. (2004). Cyclin C/Cdk3 Promotes Rb-Dependent G0 Exit. *Cell* **117**, 239-251. doi:10.1016/S0092-8674(04)00300-9

Saldanha, A. J. (2004). Java Treeview – extensible visualization of microarray data. *Bioinformatics* **20**, 3246-3248. doi:10.1093/bioinformatics/bth349

Sangrar, W., Gao, Y., Scott, M., Truesdell, P. and Greer, P. A. (2007). Fer-mediated cortactin phosphorylation is associated with efficient fibroblast migration and is dependent on reactive oxygen species generation during integrin-mediated cell adhesion. *Mol. Cell. Biol.* **27**, 6140-6152. doi:10.1128/MCB.01744-06

Sarayloo, F., Spiegelman, D., Rochefort, D., Akçimen, F., Oliveira, R. D. B., Dion, P. A. and Rouleau, G. A. (2020). SKOR1 has a transcriptional regulatory role on genes involved in pathways related to restless legs syndrome. *Eur. J. Hum. Genet.* **28**, 1520-1528. doi:10.1038/s41431-020-0670-4

Schackmann, R. C., Van Amersfoort, M., Haarhuis, J. H., Vlug, E. J., Halim, V. A., Roodhart, J. M., Vermaat, J. S., Voest, E. E., Van Der Groep, P., Van Diest, P. J. et al. (2011). Cytosolic p120-catenin regulates growth of metastatic lobular carcinoma through Rock1-mediated anoikis resistance. *J. Clin. Invest.* **121**, 3176-3188. doi:10.1172/JCI41695

Takaesu, N. T., Stinchfield, M. J., Shimizu, K., Arase, M., Quijano, J. C., Watabe, T., Miyazono, K. and Newfeld, S. J. (2012). Drosophila CORL is required for Smad2-mediated activation of Ecdysone Receptor expression in the mushroom body. *Development* **139**, 3392-3401. doi:10.1242/dev.079442

Takeshima, H., Shimuta, M., Komazaki, S., Ohmi, K., Nishi, M., Iino, M., Miyata, A. and Kangawa, K. (1998). Mitsugumin29, a novel synaptophysin family member from the triad junction in skeletal muscle. *Biochem. J.* **331**, 317-322. doi:10.1042/bj3310317

Tavares, S., Liv, N., Pasolli, M., Opdam, M., Rätze, M. A. K., Saornil, M., Sluimer, L. M., Hengeveld, R. C. C., Van Es, R., Van Werkhoven, E. et al. (2022). FER regulates endosomal recycling and is a predictor for adjuvant taxane benefit in breast cancer. *Cell Reports* **39**, 110584. doi:10.1016/j.celrep.2022.110584

Tecalco-Cruz, A. C., Ríos-López, D. G., Vázquez-Victorio, G., Rosales-Alvarez, R. E. and Macías-Silva, M. (2018). Transcriptional cofactors Ski and SnoN are major regulators of the TGF-β/Smad signaling pathway in health and disease. *Signal Transduct. Target. Ther.* **3**, 15. doi:10.1038/s41392-018-0015-8

Teo, K., Gómez-Cuadrado, L., Tenhagen, M., Byron, A., Rätze, M., Van Amersfoort, M., Renes, J., Strengman, E., Mandoli, A., Singh, A. A. et al. (2018). E-cadherin loss induces targetable autocrine activation of growth factor signalling in lobular breast cancer. *Sci. Rep.* **8**, 15454. doi:10.1038/s41598-018-33525-5

Tinevez, J.-Y., Perry, N., Schindelin, J., Hoopes, G. M., Reynolds, G. D., Laplantine, E., Bednarek, S. Y., Shorte, S. L. and Eliceiri, K. W. (2017). TrackMate: An open and extensible platform for single-particle tracking. *Methods* **115**, 80-90. doi:10.1016/j.ymeth.2016.09.016

Van De Ven, R. A. H., Tenhagen, M., Meuleman, W., Van Riel, J. J. G., Schackmann, R. C. J. and Derksen, P. W. B. (2015). Nuclear p120-catenin regulates the anoikis resistance of mouse lobular breast cancer cells through Kaiso-dependent Wnt11 expression. *Dis. Model. Mech.* **8**, 373-384. doi:10.1242/dmm.018648

Wu, J.-W., Krawitz, A. R., Chai, J., Li, W., Zhang, F., Luo, K. and Shi, Y. (2002). Structural Mechanism of Smad4 Recognition by the Nuclear Oncoprotein Ski Insights on Ski-Mediated Repression of TGF-β Signaling. *Cell* **111**, 357-367. doi:10.1016/S0092-8674(02)01006-1

Yakymovych, I., Yakymovych, M. and Heldin, C.-H. (2017). Intracellular trafficking of transforming growth factor β receptors. *Acta Biochim. Biophys. Sin.* **50**, 3-11. doi:10.1093/abbs/gmx119

Yoneyama, T., Angata, K., Bao, X., Courtneidge, S., Chanda, S. K. and Fukuda, M. (2012). Fer kinase regulates cell migration through α-dystroglycan glycosylation. *Mol. Biol. Cell* **23**, 771-780. doi:10.1091/mbc.e11-06-0517

Yu, L., Liu, X., Cui, K., Di, Y., Xin, L., Sun, X., Zhang, W., Yang, X., Wei, M., Yao, Z. et al. (2015). SND1 acts downstream of TGFβ1 and upstream of smurf1 to promote breast cancer metastasis. *Cancer Res.* **75**, 1275-1286. doi:10.1158/0008-5472.CAN-14-2387

Zheng, Y., Sethi, R., Mangala, L. S., Taylor, C., Goldsmith, J., Wang, M., Masuda, K., Carrami, E. M., Mannion, D., Miranda, F. et al. (2018). Tuning microtubule dynamics to enhance cancer therapy by modulating FER-mediated CRMP2 phosphorylation. *Nat. Commun.* **9**, 476. doi:10.1038/s41467-017-02811-7

Zirngibl, R., Schulze, D., Mirski, S. E., Cole, S. P. and Greer, P. A. (2001). Subcellular localization analysis of the closely related Fps/Fes and Fer protein-tyrosine kinases suggests a distinct role for Fps/Fes in vesicular trafficking. *Exp. Cell Res.* **266**, 87-94. doi:10.1006/excr.2001.5217